Sedimentology and chronology of the advance and retreat of the last British-Irish Ice Sheet on the continental shelf west of Ireland

Jared L. Peters[1]*, Sara Benetti[1], Paul Dunlop[1], Colm Ó Cofaigh[2], Steven G. Moreton[3], Andrew J. Wheeler[4], Christopher D. Clark[5]

[1] *School of Geography and Environmental Sciences, University of Ulster, Cromore Road, Coleraine, BT52 1SA, Northern Ireland, UK*

[2] *Department of Geography, Durham University, Durham, DH1 3LE, UK*

[3] *Natural Environment Research Council, Radiocarbon Facility, East Kilbride, Scotland, G75 OQF*

[4] *School of Biological, Earth and Environmental Sciences, University College Cork, Cork, Ireland*

[5] *Department of Geography, University of Sheffield, Sheffield, S10 2TN, UK*

* *Corresponding author; email: Peters-J@email.ulster.ac.uk*

Abstract

The last British-Irish Ice Sheet (BIIS) had extensive marine-terminating margins and was drained by multiple large ice streams and is thus a useful analogue for marine-based areas of modern ice sheets. However, despite recent advances from investigating the offshore record of the BIIS, the dynamic history of its marine margins, which would have been sensitive to external forcing(s), remain inadequately understood. This study is the first reconstruction of the retreat dynamics and chronology of the western, marine-terminating, margin of the last (Late Midlandian) BIIS. Analyses of shelf geomorphology and core sedimentology and chronology enable a reconstruction of the Late Midlandian history of the BIIS west of Ireland, from initial advance to final retreat onshore. Five AMS radiocarbon dates from marine cores constrain the timing of retreat and associated readvances during deglaciation. The BIIS advanced without streaming or surging, depositing a bed of highly consolidated subglacial traction till, and reached to within ~20 km of the shelf break by ~24,000 Cal BP. Ice margin retreat was likely preceded by thinning, grounding zone retreat and ice shelf

formation on the outer shelf by ~22,000 Cal BP. This ice shelf persisted for ≤2,500 years, while retreating at a minimum rate of ~24 m/yr and buttressing a >150-km long, 20-km wide, bathymetrically-controlled grounding zone. A large (~150 km long), arcuate, flat-topped grounding-zone wedge, termed here the Galway Lobe Grounding-Zone Wedge (GLGZW), was deposited below this ice shelf and records a significant stillstand in BIIS retreat. Geomorphic relationships indicate that the BIIS experienced continued thinning during its retreat across the shelf, which led to increased topographic influence on its flow dynamics following ice shelf break up and grounding zone retreat past the GLGZW. At this stage of retreat the western BIIS was comprised of several discrete, asynchronous lobes that underwent several readvances. Sedimentary evidence of dilatant till deposition suggests that the readvances may have been rapid and possibly associated with ice streaming or surging. The largest lobe extended offshore from Galway Bay and deposited the Galway Lobe Readvance Moraine by <18,500 Cal BP. Further to the north, an ice lobe readvanced at least 50 km offshore from Killary Harbour, possibly by ≤15,100 Cal BP. The existing chronology currently does not allow us to determine conclusively whether these readvances were a glaciodynamic (internally–driven) response of the ice sheet during deglaciation or were climatically-driven. Following the <18,500 Cal BP readvance, the Galway Lobe experienced accelerated eastward retreat at an estimated rate of ~113 m/yr.

Key words

British-Irish Ice Sheet; retreat rate; grounding zone wedge; readvance; radiocarbon; sedimentology; geomorphology; ice shelf; Killard Point Stadial; Nahanagan (Younger Dryas) Stadial

1. Introduction

Marine-terminating sectors of large ice sheets are considered to be potentially inherently unstable and sensitive to climatic and ocean forcing(s) (Cook et al., 2005; Rignot et al., 2010; Glasser et al., 2011). Palaeo-glaciological data in the form of glacial geology and geomorphology is increasingly used to constrain numerical ice sheet models of present and future ice sheet change (e.g. Bentley et al., 2010; Robinson et al., 2011; Lecavalier et al., 2014). A logical step towards improved model accuracy will come from advancing our knowledge of previous ice sheet behaviour along marine-terminating margins. By developing a thorough understanding of ice sheet behaviour during the Pleistocene, from maximum extent to final retreat, palaeoglaciological assessments enable improved understanding of the controls on modern ice sheet dynamics and provide a means of testing the veracity of predictive models. The last British-Irish Ice Sheet (BIIS) is a potential analogue for marine-based ice sheet retreat because it consisted largely of marine-based (~300,000 km^3) ice with termini fed by ice streams and flanked by ice shelves (Clark et al., 2012a).

Ongoing efforts to reconstruct the size, dynamic behaviour and chronology of the last BIIS have recently focused on its marine-terminating margins on the continental shelves around Ireland and Britain (e.g. Bradwell et al., 2008; Ó Cofaigh et al., 2010; Peters et al., 2015). This extends from over a century of largely terrestrially-based research on the last BIIS (Clark et al., 2012a). In the south of Ireland, these efforts have extended the maximum southern position of the ice sheet (Fig. 1) hundreds of kilometres beyond previous reconstructions (Scourse et al., 1990; Ó Cofaigh and Evans, 2007; Praeg et al., 2015). Marine research north of Scotland provides sedimentary evidence for a coalescence of the BIIS with the Fennoscandian Ice Sheet (Sejrup et al., 1994) and recent analyses of bathymetric data provide evidence for grounded ice extending across the West Shetland Shelf (Bradwell et al., 2008). West of Ireland, geomorphic analyses of new bathymetric data provide compelling evidence for the extension of grounded ice to the shelf break west of the Malin Sea and Donegal Bay during the LGM and subsequent lobate readvances during deglaciation (Benetti et al., 2010; Dunlop et al., 2010; Ó Cofaigh et al., 2010; Fig. 1). Geomorphic, sedimentary and

micropaleontological analyses show that the last BIIS reached the Porcupine Bank, west of Ireland (Fig. 1), and that its behaviour there was dynamic, fluctuating in extent and forming an ice shelf over the Slyne Trough (Peters et al., 2015). These offshore studies have led to a general shift in the prevailing consensus on BIIS maximum extent from a marine margin that did not extend far past the modern western Irish coastline (Bowen et al., 1986) to one that predominantly reached the edge of the continental shelf (Clark et al., 2012; Fig. 1).

Despite recent advances in understanding of the marine-terminating sectors of the BIIS, a detailed reconstruction of their retreat behaviour that incorporates chronologically constrained marine sediment analyses has yet to be established. The aim of this study is to reconstruct the dynamic behaviour of the marine-terminating margin of the last BIS on the continental shelf west of Ireland and to provide chronological constraints on its retreat. This is achieved by presenting new sedimentary data from fourteen sediment cores (three were used in a previous study; Peters et al., 2015; Table 1) sampled from the continental shelf west of counties Mayo, Galway, Clare and Kerry, Ireland (Figs. 1, 2). Using new sedimentological data and detailed geomorphic analyses of bathymetric data, we establish a regional stratigraphy for the western Irish continental shelf that records the marine-based advance, retreat and subsequent readvances of the last BIIS (Late Midlandian; marine isotope stage 2). Five new accelerator mass spectrometer (AMS) radiocarbon dates (Table 2) provide associated chronological control including calculating retreat rates during deglaciation of the shelf.

Table 1: sediment core information.

Core	Abbreviation	Latitude (N)	Longitude (W)	Water depth (m)	Core length (m)	Reference
CE10008_35	10-35	53° 58.3809’	11° 13.7809’	269.0	0.81	This paper
CE10008_36	10-36	53° 58.3622’	11° 13.8463’	234.4	2.01	This paper
CE10008_38	10-38	53° 51.9492’	10° 42.3491’	123.5	0.81	This paper
CE10008_40	10-40	53° 40.2068’	10° 40.8039	134.8	4.0	This paper
CE10008_42	10-42	53° 46.2655’	12° 38.6542’	298.5	1.76	Peters et al. 2015
CE10008_44	10-44	53° 38.9150’	12° 16.8818’	295.1	2.30	Peters et al. 2015
CE10008_45	10-45	53° 37.7487’	12° 08.0713’	293.7	2.94	Peters et al. 2015

CE14004_36	14-36	53° 02.3689’	11° 38.1194’	155.6	1.65	This paper
CE14004_41	14-41	53° 01.0713’	10° 52.5889’	138.7	0.84	This paper
CE14004_42	14-42	52° 27.9652’	10° 59.5806’	126.0	0.81	This paper
CE14004_53	14-53	53° 23.9869’	11° 01.1200’	145.2	1.28	This paper
CE14004_54	14-54	53° 38.1163’	11° 12.5620’	174.4	1.47	This paper
CE14004_57	14-57	53° 40.2868’	10° 53.0842’	150.9	1.0	This paper
CE14004_59	14-59	53° 35.8304’	10° 37.3172’	132.0	3.43	This paper

2. Methods

This study uses singlebeam bathymetric data compiled by the Norwegian-developed Olex (www.olex.no) sonar data management software to analyse the geomorphology of the continental shelf west of Ireland. The sonar data are a compilation of voluntarily-contributed, geolocated sonar measurements and, in areas of adequate coverage, produces a raster of 5-m resolution cells that typically convey vertical data with a resolution of 1 m (www.olex.no; Bradwell et al. 2008). The bathymetric data is presented as 2D hillshaded surfaces and a series of seafloor profiles to analyse and characterise the geomorphology of glacial landforms (Fig. 2).

Fourteen vibro-cores (see Table 1) were analysed, three of which were used by Peters et al. (2015; Table 1). Cores with the designation CE10008 (Table 1) were collected during the CE10008 research cruise conducted in 2010 with the *RV Celtic Explorer*; cores labelled CE14004 were collected during the “WICPro” (West Ireland Coring Program) research cruise conducted in 2014 with the *RV Celtic Explorer*. X-radiographs of the cores were developed, usually prior to splitting, using a CARESTREAM DRX Evolution system at Ulster University, Jordanstown. The x-radiographs reveal sedimentary structures and clast or dropstone presence in the cores that may be unidentifiable from visual inspection of the core section alone. Structures visible in the x-radiographs are displayed as sketches in the sediment logs and illustrative x-radiograph examples are also provided for most lithofacies. Sediment physical properties (wet bulk density and magnetic susceptibility) were measured prior to splitting using a GEOTEK© multi sensor core logger at the National University of Ireland, Maynooth. These data are displayed in the sediment logs along with

mean values calculated for each core that allow intra-core trends to be seen and inter-core comparisons to be made. When large peaks (from individual clasts or section breaks) in the data skew the magnetic susceptibility mean, the data are smoothed by removing outlying values; the excluded measurements are highlighted in the logs. After the cores were split, sediment shear strength was measured using an Impact© shear vane, calibrated by MCC©, at intervals typically guided by lithofacies but generally ≤15 cm. Areas of high clast density or with clast-supported deposits were avoided while collecting shear strength measurements because clast contact with the vane generates spurious results.

The sediment cores were split and stored at 4°C at Ulster University, Coleraine. Visual and x-radiograph inspections, aided by physical property analyses, identified twelve lithofacies from which 1-cm slabs were subsampled. Subsampling intervals were typically guided by lithofacies descriptions (cf. Kilfeather et al., 2011), usually with at least one subsample per lithofacies and often two, which enabled improved definition of contacts and intra-lithofacies changes. A sampling interval of ≤10 cm was maintained for most of core 10-40 (the longest core examined; Table 1). Subsamples were analysed for water content, grain size and relative abundance of *Elphidium excavatum* forma *clavatum* (Feyling-Hanssen, 1972). Lithic grains >1 mm were removed by dry sieving and reported as a percent by weight of the total sediment sample. The <1 mm fraction was analysed by laser granulometry using a MALVERN Mastersizer© at Trinity College, Dublin, at intervals guided by lithofacies descriptions. In cores 10-40 and 14-59 the number of lithic grains >1 mm were counted and are displayed as number/gram of sediment (cf. Grobe, 1987), which allows a comparison to the lithic grains >1 mm reported as mass percent.

E. Clavatum specimens were identified using the morphological characteristics outlined by Feyling-Hanssen (1972). This species is used for this study because it is well-documented as an opportunistic, arctic-subarctic species that often dominates benthic foraminiferal populations in recently deglaciated marine environments (Hald et al., 1994). *E. clavatum* relative abundance is calculated as a percentage of the total number of well-preserved foraminifera tests in an aliquot.

Aliquots were split using a Green Geological© microsplitter to yield subsamples with ≥300 relatively well-preserved benthic foraminifer tests (cf. Melis and Salvi, 2009) and sieved to remove the <125 μm fraction because the sediment below this size contained very few foraminifer tests, most of which were unidentifiable, likely allochthonous fragments (cf. Peters et al., 2015). *E. clavatum* relative abundances reported by Peters et al., (2015) are referred to for core 10-45 and were produced from aliquots with ≥200 benthic foraminifer tests.

Five calcareous biogenic samples were collected for AMS radiocarbon analysis from sediment horizons interpreted to record BIIS retreat or readvance across the continental shelf west of Ireland and three previously-reported ages (Peters et al., 2015) are recalibrated for use in this study. Samples were dated at the NERC Radiocarbon Facility, Scotland, and the Poznan Radiocarbon Laboratory, Poland. The dated material was unabraded and unbroken and comprised coral fragments, paired and unpaired bivalve shells and mixed benthic foraminiferal tests (sample photographs are provided in sediment logs). Results are presented as conventional radiocarbon (^{14}C BP) and calibrated (Cal BP) ages; the calibrated 2σ median results are referenced in the text. Radiocarbon ages were calibrated at 2σ confidence level with Calib©7.1 software (Stuiver and Reimer, 1993), using the Marine13 calibration dataset (Reimer et al., 2013) and with the ΔR set as 0±50 for radiocarbon ages that fall between the Younger Dryas and Heinrich 1 cold intervals (~17.0-12.0 ka BP, Broecker et al., 1989; Bond et al., 1999; Bowen et al., 2002) and a ΔR of +300±50 for radiocarbon ages that fall between Heinrich 1 and Heinrich 2 (25.0-17.0 ka BP, Dowdeswell et al., 1995).

3. Results

3.1. Geomorphology

Ridges with various morphological characteristics are found on the continental shelf offshore of counties Mayo, Galway, Clare and Kerry, Ireland (Fig. 2). The ridges on the Porcupine Bank and Slyne Trough (the westernmost ridges) are sinuous and narrow (Fig. 2a, b). These ridges were shown to have asymmetric profiles and orientations that roughly align with corrugations on a larger, north-

south trending arcuate ridge located <10 km to the east (Peters et al., 2015; Fig. 2). This large (~80 km long), corrugated, arcuate ridge on the outer continental shelf has an asymmetric profile that narrows and steepens northward to its un-corrugated northernmost extent (Figs. 2a, 3c). Its profile asymmetry is characterised by short, steep western flanks and longer eastern flanks (Fig. 3b, c). The ridge is truncated near its middle, but appears to be/have been continuous based on the arc and orientations of the discrete segments (Fig. 2a).

East (landward) of the corrugated ridge, the continental shelf is covered by a complex of bisecting (i.e. truncated) arcuate ridges (Fig. 2). These ridges have a similar, convex-seaward morphology to the corrugated ridge but have disparate radii and profiles (Figs. 2a, 3). The southernmost, largest of these ridges is poorly defined to the south and is truncated by a smaller ridge to the north (Fig 2). This large ridge is ~150 km long and up to 22 km wide (Figs. 2, 3b, c, d). It is distinctly flat-topped and reaches heights above the surrounding seafloor of up to 20 m (Fig. 3b, c, d). The western edge of this ridge (Fig. 3, bold grey line iii) is flanked by a continuous, low-relief (~11 m high, Fig. 3) landform that is also flat-topped but distinctly lower than the main ridge crest (Figs. 2, 3). East of and nested within this large ridge is a smaller arcuate ridge that is discernible in the Olex data despite its relatively poorly defined boundaries (Fig. 2a). Although it is relatively ambiguous, this smaller ridge seems to be ~120 km long and has a southern extent that reaches ~10 km farther south than the poorly-defined southern margin of the larger, flat-topped ridge (Fig. 2a).

North of the large, flat-topped ridge are two smaller (~40–45 km long) arcuate ridges (Fig. 2). The smallest (i.e. tightest radius) of these ridges is situated between the large, flat-topped ridge and the northernmost ridge and appears to truncate both of the neighbouring landforms (Fig. 2a). This small ridge is situated east (landward) of the flat-topped, low-relief landform that flanks the large ridge. The small ridge is ~20 m tall and reaches ~106 mbsl in height, making it the bathymetrically highest ridge in the study area (Fig. 3a). It is asymmetric and is characterised by relatively steep western side but gentle eastern side (Fig. 3a). The northernmost ridge has a wider radius and is truncated by the small ridge but is otherwise geomorphically similar (Fig. 2a, d).

Much of the seafloor on the continental shelf is furrowed, particularly areas shallower than ~350 mbsl located west of the large, flat-topped arcuate ridge and in the Slyne Trough (Figs. 2, 3d). The furrows are abundant on the continental shelf in areas approximately <220 mbsl and cover both the arcuate ridges and the surrounding seafloor (Fig. 2b, c, d, e). The largest and deepest furrows occur in the Slyne Trough (Figs. 2b, c, 3d), where they have depths of >10 m and terminate against bathymetric highs (Peters et al., 2015). The furrows in the Slyne Trough often have relatively poorly defined southern termini and distinct, kettle-like depressions or pits at their northern termini (Fig. 2c, d). Some of the large Slyne Trough furrows have corrugations at their base (Fig. 2c) and are flanked by berms (Fig. 3d).

3.2. Sedimentology

Twelve lithofacies are identified by visual inspection, x-radiograph analysis (Fig 4) and sediment physical property measurements. These lithofacies are built into four lithofacies associations as described in the following subsections.

3.2.1. LFA 1: Diamicton (Dmm_c, Dmm and Dms) and compact, deformed mud (Fm and Fl(s))

Highly consolidated diamicton (Dmm_c) with shear strengths from 50 to 197 kPa (note 197 kPa is the shear vane's maximum measureable stress and thus measurements at this value are regarded as minima) was recovered at the base of six cores (10-38, 10-42, 10-44, 14-36, 14-42, 14-53) and ranges from at least 35-70 cm in thickness (Fig. 5). This sediment consists of small to large pebble-sized clasts with variable roundness supported by a matrix of muddy sand or sandy mud with up to 64% sand in 10-42 and 14% sand in 14-36 (Fig. 5). The matrix is grey or nearly black in colour (2.5Y 6/2, 2.5Y 5/2, 5Y 3/1, 5Y 2.5/1). Occasionally clasts show a preferential alignment in x-radiographs with clast a-axes oriented ~40° from horizontal (Fig. 4a). This lithofacies is characterised by high wet bulk densities (≥2.1 g/cm^3), low water content (typically <15% and as low as 2.26% in core 10-38) and low magnetic susceptibility (~13-21 10^{-8} SI)—with the exception of core 14-42 (the southernmost core), which reaches 107 10^{-8} SI (Fig. 5).

In core 10-44 a well preserved coral fragment (*Lophelia pertusa*) was recovered from the Dmm_c lithofacies. However, in cores 10-38 and 14-36 this diamicton contains little or no observed biogenic material (Fig. 5). Farther offshore (i.e. farther west), in cores 10-42 and 10-44 the Dmm_c lithofacies contains highly abraded or broken foraminifer tests but little to no poorly preserved macrofaunal test material.

The base of cores 10-35, 10-40, 14-57 and 14-59 is composed of at least 15-302 cm of poorly sorted, matrix-supported diamicton with moderate consolidation (30-50 kPa) (Fig. 5). The same diamicton overlies the Dmm_c lithofacies in cores 14-36 and 14-53, where it has a gradational lower contact (Fig. 5). The diamicton is typically massive (Dmm) with the exception of crude stratification (Dms) visible on x-radiographs at the base of cores 10-35 and 14-57 (Figs. 4, 5). The beds within the Dms lithofacies are poorly defined and are ~3 cm thick (Fig. 4g). Sandy, vertically oriented intrusions that are devoid of shell fragments extend from 0.81-1.0 m bsf of core 14-53 and yield distinctly lower shear stress values (Fig. 5). Small to large pebble sized clasts of variable roundness are common in this lithofacies and occasionally clasts are rhythmically concentrated in ~5-cm thick intervals (Fig. 4c). One 4-cm long (a-axis), sub-rounded, dark blueish grey (Gley 2, 4/5PB), fine-grained clast sampled from 3-m bsf in core 10-40 (Fig. 5) was found to have multiple sets of striations. Grain-size analyses reveal highly variable mass percentages of >1 mm grains, ranging from almost no grains in core 14-36 to >85% in core 10-40 (Fig. 5). Sand, silt and clay percentages in the matrix are also variable but typically dominated by silt or sandy silt; sand percentages commonly increase upwards (Fig. 5). In core 10-35, on the outer shelf (Fig. 2a), the Dmm lithofacies is greyish brown (2.5Y 5/2 or 2.5Y 4/2) and often sandier than the diamicton sampled from other parts of the shelf (Fig. 5). In cores 10-40, 14-36, 14-57 and 14-59 the moderately stiff diamicton is grey to very dark grey (2.5Y 5/1 to 5Y 3/1). This lithofacies is characterised by highly variable wet bulk densities (1.7-2.4 g/cm^3) and irregular water content that ranges from 4-19% (often covering a similar range within one core, Fig. 5). The Dmm lithofacies sampled from west of the large arcuate ridges (Fig. 2a) has lower magnetic susceptibility values (<36 10^{-8} SI; Fig. 5) than those recorded from east of the ridges (>90-181 10^{-8} SI; Fig. 5).

Foraminiferal tests are rare within the moderately-consolidated Dms lithofacies and are usually abraded and broken. Benthic foraminifera populations in this lithofacies are characterised by high percentages of *E. clavatum* ranging up to 65% in core 14-59 (Fig. 5).

The base of cores 10-36, 14-41 and 14-54 consists of consolidated (≥50 kPa) laminated mud lithofacies (Fl). Similar consolidated Fl and massive mud (Fm) lithofacies overlie diamictons at the base of cores 14-53 and 14-57 (Fig. 5). The mud is typically laminated (Fl) but at the base of core 10-36 it is massive (Fm); these lithofacies are further refined based on the presence of dropstones and shear planes, which are henceforth abbreviated -(d) and -(s) in the lithofacies abbreviations, respectively, following the codes established by Eyles et al. (1983). Deformed Fl lithofacies are also interbedded in the Dmm diamicton of core 14-59. Grain-size analysis of this lithofacies typically reveals small percentages (<1.5%) of >1 mm lithic grains and in core 14-41 no clasts were detected. However at the base of core 14-54 there is a peak of >1 mm grains that represents 14.5% of the sediment (by weight) and in cores 10-36, 14-54 and 14-57 large, randomly oriented lonestones are commonly observed (Fig. 5). Lonestone abundance decreases upwards through the mud lithofacies in cores 10-36 and 14-54. The mud is well sorted and silty with mean percentages of sand, silt and clay in cores 10-36, 14-41, 14-54 and 14-57 approximately 16%, 55% and 29%, respectively (Fig. 5). The mud is greyish brown to greenish black in colour (2.5Y 5/2, 2.5Y 4/1, Gley 1 2.5/10Y). Shear stress values range from moderate to high (22-80 kPa) and typically decrease upwards through the cores (Fig. 5). This lithofacies is characterised by relatively high wet bulk densities (~2.1 g/cm^3), moderate water content (14-19.8%) and typically high magnetic susceptibility (~62-90 10^{-8} SI) in cores 14-41, 14-53, 14-54 and 14-57. The westernmost occurrence of this lithofacies, in core 10-36 (Table 1, Fig. 2a), has a markedly lower magnetic susceptibility of 11 10^{-8} SI (Fig. 5).

Shear planes are common in the compact muds and displacement of laminae records both extensional and compressional strain (Fig. 4d, e). Compressional strain (thrust faulting) is only identified in compact mud with shear strength values >50 kPa. Compressional deformation in compact Fl sediment from core 14-41 can be seen in x-radiographs to have a displacement of >2 cm

along a shear plane tilted 40° from horizontal (Fig. 4e). Clasts proximal to the shear planes occasionally show preferential a-axis alignment parallel to the plane (Fig. 4d, e). In core 14-59 the Fl lithofacies consists of rhythmic, ~1 cm thick, sandy laminae with sharp lower contacts that fine upwards to mud; these laminae are deformed and show distinct inhomogeneous ductile folding (Benn and Evans, 1996; Fig. 4b).

The benthic foraminiferal population in the consolidated mud lithofacies of cores 10-36, 14-53 and 14-54 contains high percentages (relative abundance up to 38%) of well-preserved tests of *Elphidium excavatum* forma *clavatum* (Feyling-Hanssen, 1972) (Fig. 5). However this lithofacies is otherwise poor in biogenic material and in several locations (cores 14-41 and 14-57), no benthic foraminifera tests were identified in this lithofacies. In cores 14-41 and 14-57 the stiff mud is devoid of shell fragments and very few foraminifer tests were discovered (Fig. 5).

3.2.3. LFA 2: Loose diamicton (Dmm) and mud (Fl(d), Fm)

Massive, muddy diamicton (Dmm) with moderate to low shear strengths (~5-40 kPa, typically <20 kPa) occupies the base of core 10-45 and overlies the consolidated and deformed sediment of LFA 1 in cores 10-35, 10-40, 10-42, 10-44, 14-36, and 14-59 (Fig. 5). This sediment is lithologically and structurally similar to the underlying, consolidated diamicton, but is less compact and often has a higher water content and lower density than the basal deposits (Fig. 5). Like the underlying, moderately consolidated diamictons, the loose Dmm lithofacies contain variable amounts of pebble-sized clasts that comprise several lithologies. The loose Dmm contains higher amounts of sand than the underlying diamictons and the sand content typically increases up core (Fig. 5). There is a distinct decrease in the number of lithic grains >1 mm in core 10-40 between 2.05 m bsf and 1.92 from 91.3 grains/g to 1.7 grains/g; this decrease roughly correlates with a drop in the mass percentage of >1 mm grains (Fig. 5). In cores 10-35 and 10-45 (on the outer shelf; Fig. 2a) the loose Dmm lithofacies is characteristically greyish brown (2.5Y 5/2 or 2.5Y 4/2) and often sandier than the diamicton sampled from other parts of the shelf (Fig. 5).

The benthic foraminifera population of the loose Dmm lithofacies contains high amounts of *E. clavatum*, including the highest percentage observed in the analysed cores (73%, core 10-40; Fig. 5). The loose Dmm lithofacies typically contains more shell fragments than the underlying diamictons and the abundance of shell fragments often increases upwards (Fig. 5). Visual inspection reveals vertical to sub-vertical, sandy, granule and shell-fragment rich irregularities that commonly extend downwards into the top of the Dmm diamicton from the overlying lithofacies.

Loose to moderately-consolidated (20-50 kPa) mud lithofacies overlies consolidated mud lithofacies in cores 10-36, 14-41, 14-54, and 14-57 (Fig. 5). The loose or moderately-consolidated mud lithofacies are typically laminated (Fl) but massive in core 10-36. This sediment is lithologically and structurally similar to the underlying, consolidated mud deposits, but is less compact and usually has a higher water content and lower density than the basal deposits (Fig. 5). Lonestones of variable lithologies are common in this lithofacies, but are typically less abundant than in the underlying mud deposits and often decrease in abundance up core (Fig. 5). Shear planes are common in the loose mud lithofacies in cores 14-41, 14-54 and 14-57 (Fig. 5). At ~0.5 m bsf in core 14-54 the loose Fl(s) lithofacies contains an unconsolidated, sandy, soft-sediment clast (Fig. 5).

The benthic foraminifera population of the loose mud lithofacies is dominated by *E. clavatum* and reaches relative abundances from 30% to 38% (Fig. 5). Vertical to sub-vertical, sand and shell-fragment rich irregularities commonly extend downwards into the top of the loose mud lithofacies from the overlying deposits (Fig. 5).

3.2.4. LFA 3: Coarse, clast-supported lithofacies (Dcm, GO) and shell hash (SH and GSH)

Coarse, massive, clast-supported diamicton (Dcm) or openwork gravel (GO) overlies the muddy and diamictic lithofacies of LFA 1 and LFA 2 in eight of the cores examined in this study (10-35, 10-38, 10-42, 10-44, 10-45, 14-42, 14-57, 14-59). These facies are relatively thin, ranging from 5 to 25 cm in thickness (Fig. 5). Lower contacts are typically diffuse, except above the Dmm_c lithofacies in core 10-38, the Fl(s) lithofacies in core 14-57 and the Dmm lithofacies in core 14-59

(Fig. 5). This lithofacies consists of small to large pebble-sized clasts of variable lithologies and roundness, surrounded by varying amounts of coarse sandy matrix. A clast in the Dcm facies in core 10-45 exhibited striations, a "rounded nose" and a "plucked lee" (Peters et al., 2015; Fig. 5). In core 10-38, the Dmm_c lithofacies is overlain by GO gravel with rare granules occupying the inter-pebble cavities (Fig. 4h). Grain-size analyses reveal moderate to high percentages of lithic fragments >1 mm (typically >20% and up to 46% in core 10-45, Fig. 5). Matrix material is dominated by sand (>60-90%) and typically contains shell fragments. The colour of this lithofacies is highly variable, but the matrix is often similar in colour to the underlying diamicton; conversely, in cores 10-38, 14-57 and 14-59 (where these lithofacies have sharp lower contacts), the GO and Dcm matrix material is more similar to the overlying sediment. This lithofacies is characterised by high wet bulk densities (up to 2.5 g/cm^3 in cores 10-35 and 14-59), low water content (13.5-14.5%) and highly variable magnetic susceptibility, often with irregular peaks above or below the core mean (Fig. 5).

The foraminifera sampled from the matrix material of the Dcm facies were often broken and abraded (cf. Peters et al., 2015). Well preserved *E. clavatum* are rare in the Dcm sediment (>5% relative abundance), but occasionally high numbers were are recovered in the surrounding deposits (31.1-44.8% relative abundance in core 14-59, Fig. 5). Shell fragments are common in the Dcm and GO lithofacies and lower contacts are commonly bisected by poorly-sorted, vertical to sub-vertical, sandy, granule and shell-fragment rich inclusions.

A shell hash (SH) or gravelly shell hash (GSH) consisting primarily of highly fragmented bivalve shells overlies the diamictic and muddy lithofacies in cores 10-40, 14-41, 14-53, 14-54, 14-59 (Fig. 5). This lithofacies has both diffuse and sharp lower contacts and varies from 7-148 cm in thickness (Fig. 5). The shell hash occurs most commonly and typically with the greatest thickness in the easternmost cores. Rounded, pebble sized clasts of variable lithologies are common in the GSH deposits in cores 10-40 and 14-41 (Fig. 5). Grain-size analyses of the <1 mm sediment fraction of the SH lithofacies in core 14-59 reveal the small amounts of matrix sediment to be 100% sand (Fig. 5). In core 10-40, the GSH sediment contains a high percentage of granules >1 mm (64.5-80.8%, Fig. 5).

The colour of this lithofacies is variable, but typically light yellowish brown to light olive brown (2.5Y 6.4 to 2.5Y 5/6). This lithofacies is characterised by highly variable wet bulk densities with erratic peaks that usually fall well above the core mean, magnetic susceptibility values below the core mean, low shear stress measurements (<6 kPa), and low water content (<17.3%, typically <7% and as low as 3.9% in core 10-40, Fig. 5).

The foraminifera sampled from the sand matrix of the shell hash deposits were often broken and abraded. The indicator species *E. clavatum* is relatively rare in the SH and GSH lithofacies and shows an upwards decrease in abundance (e.g. cores 10-40 and 14-59, Fig. 5). In cores 14-41 and 14-54, lower contacts are bisected by vertical to sub-vertical sandy, granule and shell-fragment rich irregularities.

3.5.6. LFA 4: Sandy lithofacies (Sh, Suf, Sm)

The top of each of the cores analysed for this study, with the exception of core 14-59 (the easternmost core), is composed of massive (Sm), upward fining (Suf) or crudely horizontally bedded sand (Sh) lithofacies; the sand is 6-50 cm thick and usually has sharp lower contacts (Fig. 5). These lithofacies are well sorted with grain-size analyses revealing very high amounts of sand (up to 94% in core 14-41, Fig. 5). The sandy deposits from the westernmost cores (10-35, 10-36, 10-42, 10-44) are greyish brown (2.5Y 5/2); in the remaining cores, the sand is light yellowish brown (2.5Y 6/3) to olive yellow (2.5Y 6/6) in colour. This lithofacies is characterized by low wet bulk densities (often <2.0 g/cm^3) that decrease upwards, low shear strengths (<5 kPa), moderate to high water contents (usually >20%) that increase upwards, and often low magnetic susceptibility values (usually <40 10^{-8} SI) that are less than core mean values (Fig. 5). Moderate magnetic susceptibility values from ~62 to as much as ~70 10^{-8} SI are recorded from cores 14-41, 14-42, 14-54, 14-57 and 14-59 (the easternmost cores, Fig. 2a).

The sand lithofacies yielded few *E. clavatum* tests, often with no individuals found near the core tops (Fig. 5). Shell fragments are abundant near the bottom of these lithofacies, but usually

decrease in size and occurrence upwards (e.g. 20-5 cm bsf in core 10-35, Fig. 4j). Irregularly shaped areas of relatively low density, composed of poorly-sorted, shell-fragment rich material are common (Fig. 4j).

3.4. Chronology

Five samples of calcareous, marine biogenic material were dated using AMS radiocarbon analyses (Table 2). All samples were well preserved, with little to no abrasion, breakage or discolouration. The samples were taken from glacigenic material collected on the continental shelf. Three AMS radiocarbon ages from a previous study (Peters et al., 2015) on the Porcupine Bank and Slyne Trough are also recalibrated for use in this study (Table 2). The oldest age on the shelf west of Ireland (24,067 Cal BP) is sampled from core 14-44 in the Slyne Trough (one of the westernmost cores). The age distribution across the shelf reveals a typical eastward trend of younger sediment deposition, with the youngest age of 15,148 Cal BP from the easternmost core (14-59, Table 2).

Table 2: Radiocarbon ages from the western Irish continental shelf.

Core	Depth (cm bsf)	Sample material	^{14}C age (yrs. BP)	ΔR used	Calibrated 2σ age range (yrs. BP)	Calibrated 2σ age median (yrs. BP)	δ^{13}C (‰)	Laboratory code
10-35	45	Paired bivalve shell	18,060±120	+300±50	21,339-20,588	20,944	8.5	UCIAMS-144579
10-42	36	Paired bivalve shell	17,900±89*	+300±50	21,034-20,470	20,741	-4.7	Poz-66484
10-44	75	Coral fragment	13,614±48	0±50	16,109-15,646	15,876	-6.5	SUERC-48915
10-44	180	Coral fragment	20,710±90*	+300±50	24,351-23,783	24,067	-1.3	Beta-334419
10-45	94	Single bivalve shell	18,733±107*	+300±50	22,210-21,504	21,841	4.3	Poz#2-66430
14-53	70	Mixed benthic foraminifera	15,956±87	+300±50	18,748-18,280	18,517	-6.9	Poz-66485
14-54	134	Mixed benthic foraminifera	18,222±59	+300±50	21,437-20,891	21,161	-1.0	SUERC-58294
14-59	325	Single bivalve shell	13,121±42	0±50	15,349-14,844	15,148	-0.1	SUERC-58295

* From Peters et al., 2015.

4. Interpretation

4.1. Geomorphology

4.1.1. Seafloor ridges

The arcuate and nested shapes, scale and orientation of the seafloor ridges are inconsistent with the regional, bedrock-controlled geomorphic trends discernible in the topographic DEM (Fig. 2a), but they are comparable to submerged moraines (e.g. Bradwell et al., 2008; Ó Cofaigh et al., 2010). This suggests that the ridges are likely formed in association with marine-terminating ice margins during glacial advance or retreat on the shelf. The asymmetrical profile and arcuate shape of the westernmost corrugated ridge (Figs. 2a, b, 3b, c) is consistent with deposition as a push moraine with a steep ice-distal flank to the west (Boulton, 1986). The corrugations on its southern end are aligned with the sinuous ridges in the Slyne Trough, which have been interpreted as a record of grounded ice extent, followed by ice shelf recoupling during retreat (Peters et al., 2015). The ridge-corrugation alignment (Fig. 2b) suggests that the corrugations may have been formed contemporaneously and by the same mechanism as the ridges in the Slyne Trough. Thus we tentatively interpret the arcuate ridge to be a push moraine that was subsequently overridden by an ice shelf that extended over the Slyne Trough (Peters et al., 2015). This interpretation is supported by the southward broadening of the arcuate ridge, which is consistent with moraines that were overridden and smoothed by readvancing ice (e.g. Bentley et al., 2007; Jónsson et al., 2014). This partially overridden, westernmost arcuate ridge is henceforth referred to as the West Ireland Moraine (WIM).

The arcuate shape of the largest, southernmost ridge in the study area (Fig. 2a) is consistent with ice-marginal deposition against BIIS marine termini (cf. Bradwell et al., 2008; Ó Cofaigh et al., 2010). Its flat-topped profile (Fig. 3b, c) suggests deposition below a floating ice mass that constrained vertical accretion (Dowdeswell et al., 2008; Batchelor and Dowdeswell, 2015). Thus, we interpret this landform as a grounding-zone wedge that formed against an ice lobe with a floating ice shelf. Because of the location of the ridge on the continental shelf, we interpret the ice lobe to have most likely emanated from south of the Maumturk Mountains, roughly centred on Galway Bay (Fig. 2a); thus, this feature is henceforth referred to as the Galway Lobe Grounding-Zone Wedge

411 (GLGZW). The low-relief, flat-topped landform that forms the western flank of the GLGZW (Figs. 2,
412 3) is interpreted to most likely record an earlier phase of grounding-zone wedge deposition because of
413 its geomorphic similarities to the GLGZW. Therefore, we interpret both flat topped landforms to be
414 components of a complex, grounding zone deposit that was built under ice shelves with variable
415 thicknesses along an apparently bathymetrically controlled grounding zone (cf. Ó Cofaigh et al.,
416 2005). The dimensions of the GLGZW (~150 km long and 22 km wide) are similar to some large
417 Antarctic grounding-zone wedges (Evans et al., 2005) and indicate that it likely records a significant
418 (i.e. centuries long) stillstand during BIIS retreat (cf. Dowdeswell et al., 2008).

419 The ridge situated directly east of the GLGZW (Fig. 2a) is interpreted to most likely be a
420 recessional or readvance moraine based on its smaller size and nested relationship to the larger ridge
421 (cf. Ó Cofaigh et al., 2010). Because of its similar orientation, which is indicative of ice extension
422 roughly from Galway Bay, this moraine was likely formed by ice draining a similar area to the
423 GLGZW. Thus, this moraine is henceforth referred to as the Galway Lobe Readvance Moraine.
424 However, the term 'readvance' is used tentatively on the basis of only the geomorphic evidence.

425 The two arcuate ridges north of the GLGZW have steep, asymmetric flanks (Figs. 2, 3a)
426 consistent with deposition as push moraines (Boulton, 1986). The smaller, southern ridge truncates
427 the GLGZW and the northern ridge, indicating that it likely formed during ice overriding of the
428 surrounding landforms following their deposition. Based on their relatively close proximity to land
429 (within ~25 km, Fig. 2a), their well-preserved, steep-sided morphology, and cross-cutting nature of
430 these ridges, they are interpreted to have been formed during the readvance of ice lobes across the
431 shelf (cf. Bradwell et al., 2008). The smaller, evidently younger ridge is henceforth referred to as the
432 Connemara Lobe Moraine because it is positioned offshore of the mountainous Connemara district
433 (Fig. 2a). The arcuate ridge situated north of the Connemara Lobe Moraine is interpreted as an older
434 recessional or readvance moraine that likely extended onto the shelf from ice sources that drained past
435 Clew or Blacksod bays from County Mayo based on its geographic position (Figs. 1, 2a). This
436 landform is henceforth referred to as the Mayo Lobe Moraine.

437 *4.1.2. Seafloor furrows*

438 The seafloor furrows are interpreted as iceberg scours based on their irregular, occasionally
439 meandering, trajectories and the presence of adjacent lateral berms (Belderson et al., 1973;
440 Dowdeswell et al., 1993; Ó Cofaigh et al., 2002, 2010; Fig. 3d). Their abundance on the shelf in
441 water depths approximately <350 mbsl suggests a local iceberg source and supports an interpretation
442 of ice shelf formation and subsequent break up west of the GLGZW (Peters et al., 2015). When
443 identified, the gradual scour termini mark the deepest water depths of the scours and the abrupt, pit-
444 like depressions mark the shallowest points (cf. Andreassen et al., 2014; Fig. 2c). Thus, the gradual
445 and abrupt termini are interpreted to record the inception of iceberg contact with the seafloor and
446 iceberg grounding pits, respectively (cf. Hill et al., 2008; Andreassen et al., 2014). The abrupt scour
447 termini in the Slyne Trough are typically located at the northern ends of the scours, indicating a
448 northward or northeastward palaeocurrent (cf. Peters et al., 2015) or a combination of current and
449 wind interaction. The corrugated troughs that characterise some scours are interpreted as the
450 signature of tidal action on the grounded icebergs (cf. Jakobsson et al., 2011). Rare parallel furrows
451 (Fig. 2c, d) indicate the grounding of large icebergs with multiple keels and suggests calving from a
452 collapsing ice shelf (Andreassen et al., 2014).

453 ***4.2. Sedimentology***

454 Four Lithofacies Associations (LFAs) are identified in the cores and record the sedimentary
455 history from BIIS advance to Holocene postglacial marine sedimentation. Without sub-bottom
456 seismic stratigraphic data, these lithofacies are assumed to sample the glacial landform-creating
457 sediment in cores 10-35, 10-38, 10-40, 10-42, 10-44, 10-45, 14-36, 14-42, 14-54, 14-57 and 14-59
458 because of their penetration depths (up to 4.0 m) and close proximity (usually in contact with,
459 occasionally ≤440 m) to the landforms (Fig. 2a). This assumption is reinforced by sedimentological
460 similarities to glacially-derived sediment described by previous studies from formerly glaciated
461 continental shelves (e.g. Ó Cofaigh and Dowdeswell, 2001; Dowdeswell et al., 2004; Evans et al.,
462 2005, Ó Cofaigh et al., 2005, 2011; Hillenbrand et al., 2010).

463 *4.2.1. Lithofacies association 1 (ice-contact deposition/reworking)*

464 LFA 1 consists of Dmm_c, Dmm, Fl(s) and consolidated or deformed Fm lithofacies. The Dmm_c
465 diamicton at the base of cores 10-38, 10-42, 10-44, 14-36, 14-42 and 14-54 (Fig. 5) is interpreted as
466 an overconsolidated subglacial traction till based on its high shear strength, massive structure, high
467 wet bulk density and low water content (cf. Wellner et al., 2001, Evans et al., 2005, Ó Cofaigh et al.,
468 2005; D. Evans et al., 2006). Striated clasts within the Dmm_c diamicton also support a subglacial
469 depositional environment (Sharp, 1982). Areas of high shear strength (50->197 kPa, Fig. 5) suggest
470 thick ice, low pore-water pressures and potentially low ice-flow velocities (non-streaming) (Sættem et
471 al., 1996; cf. Dowdeswell et al., 2004). Preferentially-oriented clast a-axes indicate alignment with
472 strain during subglacial till formation (Benn and Evans, 1996; Bennett and Glasser, 2011; van der
473 Meer et al., 2003; J. Evans et al., 2006). Microfossil damage is consistent with the cannibalisation
474 and subglacial reworking of pre-glacial marine sediment (Ó Cofaigh et al., 2011); sediment devoid of
475 foraminiferal tests suggests a terrigenous sediment supply. A coral fragment from core 10-44 is AMS
476 radiocarbon dated to 24,067 Cal BP. This date is interpreted to constrain the maximum age of the till
477 deposited during the advance of the last BIIS (Peters et al., 2015; Table 2).

478 The Dmm at the base of cores 10-35, 14-57 and 14-59 and overlying the overconsolidated basal
479 till in cores 14-36 and 14-53 (Fig. 5) is also interpreted as a subglacial traction till, associated with
480 deformation of dilatant sediment, because of its massive or crudely stratified structure and moderate
481 shear strengths that gradually decrease upwards (Benn and Evans, 1996; J. Evans et al., 2005, 2006;
482 D. Evans et al., 2006). Sandy, vertically oriented inclusions with moderate shear strength (40 kPa) in
483 core 14-53 (Fig. 5) are interpreted as dewatering structures and, along with the increase in water
484 content (up to 19%) relative to the underlying, stiff basal till, indicate higher porosity and pore-water
485 pressures (Rijsdijk et al., 1999; van der Meer et al., 1999). Furthermore, clast lithology, magnetic
486 susceptibility and foraminiferal content is comparable between the Dmm and Dmm_c lithofacies,
487 suggesting that the former is derived from the reworking of the latter (cf. Dowdeswell et al., 2004;
488 Evans et al., 2005; Kilfeather et al., 2011). An unabraided, unbroken, parasitized bivalve shell in the

till near the base (325 cm bsf) of core 14-59 (Fig. 5) is AMS radiocarbon dated to 15,148 Cal BP (Table 2). This age indicates that the ice advanced over and incorporated material that was biomineralized late in MIS 2. This suggests that either an ice mass readvanced to this point or icebergs grounded against moraines on the shelf at least 1,000 years after the Killard Point Stadial.

The highly-consolidated, silt-rich Fl(d) and Fl(s) deposits overlying the subglacial tills in cores 10-36, 14-41, 14-53, 14-54 and 14-57 are interpreted as glacitectonised glaciomarine sediment based on their preserved primary structures (laminae), thrust faults and high shear strengths (Benn and Evans, 1996). The sediments were likely originally deposited proglacially by suspension settling from sediment plumes based on their high silt content, parallel laminae and dropstones (Ó Cofaigh and Dowdeswell, 2001). Areas devoid of foraminiferal tests and with few dropstones in cores 14-41 and 14-57 support an interpretation of terrigenous sediment supply in an ice-proximal, possibly sub-ice shelf environment. These sediments were likely glacitectonised penecontemporaneously during recoupling. Conversely, glacitectonised suspension plume sediment (Fl(d) and Fl(s)) with abundant *E. clavatum* tests in cores 10-36, 14-53 and 14-54 (Fig. 5) is interpreted to have been deposited proglacially prior to being overridden (cf. Ó Cofaigh et al., 2011). The sharp lower contacts and normal grading of the folded Fl lithofacies in core 14-59 (Figs. 4b, 5) indicate a glaciomarine primary depositional environment. The laminae are interpreted as having been deposited by suspension settling from meltwater plumes (plumites) based on their rhythmic nature, sharp lower contacts and upward fining (Dowdeswell et al., 2000). The ductile, inhomogeneous folding identified in the Dms lithofacies of core 14-59 is interpreted to record compressional strain. The evidence for compressional strain and moderate shear strength (up to 28 kPa) in the folded sediment are consistent with glaciotectonisation from an overriding ice mass (Benn and Evans, 1996; Ó Cofaigh et al., 2011). An interpretation of ice readvance over these sites is supported by two AMS radiocarbon dates acquired from relatively well-preserved (i.e., light surface abrasion but little discolouration or fracturing) mixed benthic foraminifera (dominantly *E. clavatum*) that were sampled from within the glaciotectonite of cores 14-53 and 14-54 (Table 2, Fig. 5). The ages constrain the biomineralization of tests within the glaciotectonite to ≤21,161 Cal BP (core 14-54, Table 2) west of the GLGZW and

516 ≤18,517 Cal BP (core 14-53, Table 2) east of the GLGZW. These ages suggest a readvance of the ice
517 sheet across the shelf either associated with glaciodynamic adjustments during deglaciation or
518 possibly related to climate forcing during the Killard Point (Heinrich event 1) stadial (McCabe and
519 Clark, 1998; McCabe et al., 2005, 2007; Clark et al., 2009a, 2009b, 2012b, and references therein).

520 *4.2.2. Lithofacies association 2 (Glaciomarine deposition and iceberg turbation)*

521 This LFA consists of Dmm, Fl(d) and Fm lithofacies with a deposit of Sm lithofacies in core
522 14-53 (Fig. 5). The loose, greyish-brown Dmm diamicton overlying the till and glaciotectonite in
523 cores 10-35, 10-42, 10-44 and 14-36 and at the bottom of cores 10-40, 10-45 and 14-59 (Fig. 5) is
524 interpreted as the signature of meltwater-derived sediment-plume suspension settling (plumite) with
525 high IRD input (rain-out sediment) based on its low to moderate shear strength (6-25 kPa), high water
526 content, abundance of outsized lonestones, and highly variable wet bulk density and magnetic
527 susceptibility (cf. Hillenbrand et al., 2005; Lucchi et al., 2013). Similarly, the loose, greyish-brown
528 mud overlying the glaciotectonite in cores 10-36, 14-41, 14-54 and 14-57 (Fig. 5) is interpreted as
529 proglacial, retreat-phase suspension plume sediment with more meltwater-derived fines and less IRD
530 than the massive diamicton, based on its laminated structure, high silt content, moderate shear
531 strength (20-40 kPa), and variable wet bulk density and magnetic susceptibility (Dowdeswell et al.,
532 2000; Ó Cofaigh and Dowdeswell, 2001). The massive, shelly sand (Sm) from 32-49 cm bsf in core
533 14-53 is highly deformed (indicated by large areas of loose sediment or void space against the core
534 liner; Fig. 5) but tentatively interpreted as a postglacial current deposit or sandy rain-out deposit that
535 dewatered and mixed with the overlying shell hash during core acquisition. The rain-out sediment in
536 the three westernmost cores from the Slyne Trough (10-42, 10-44 and 10-45, Fig. 2a) has previously
537 been interpreted as *in situ*, sub-ice shelf and ice-proximal rain-out sediment based on
538 micropaleontological data, clast abundance and lithologic similarity (Peters et al., 2015). Variability
539 in the wet bulk density and magnetic susceptibility is interpreted as a signature of the high sediment
540 heterogeneity. The mud component in LFA 2 typically decreases upwards (Fig. 5), which is also
541 consistent with an interpretation of increasingly ice-distal glaciomarine sedimentation (cf. Smith et al.,

2011). Zones of high clast density within the cores (e.g. core 10-40, Fig. 4c) are probably related to increased delivery of IRD to the core sites and their rhythmic occurrence is likely a record of a seasonal IRD production (Cowan et al., 1997) or seasonal sea-ice cover that suppressed iceberg activity (Dowdeswell et al., 2000; Ó Cofaigh et al., 2001). This rain-out deposit is dated to ≤21,841 Cal BP (core 10-45, Table 2) in the Slyne Trough (Peters et al., 2015) and an AMS radiocarbon date from a well preserved (unbroken and unabraded), paired bivalve shell sampled from 45 cm bsf in core 10-35 (Fig. 5) provided an age of 20,944 Cal BP (Table 2). This date constrains the age of deposition for glaciomarine sedimentation and BIIS retreat from the Slyne Trough.

The genesis of plumite and rain-out sediment is further refined based on IRD abundance, secondary structures, biogenetic content, and the presence of vertical to sub-vertical shell-fragment rich sand intrusions interpreted as related to bioturbation. Grounding line-proximal sediment is identified at the base of the proglacial deposits based on high IRD abundance, a lack of bioturbation or macro-shell fragments, and a benthic foraminiferal population dominated by *E. clavatum* (cf. Lucchi et al., 2013). Conversely, grounding line-distal deposits are differentiated by the presence of unabraded bivalve shells and fragments, reduced or absent IRD sedimentation and bioturbation towards the top of the deposit (cf. Löwemark et al., 2015).

Post-depositional reworking, likely from iceberg turbation, or debris flows is identified above the till in cores 14-41, 14-42 and 14-57 and overlying the proglacial plumite in core 14-54 based on occasional shear planes and soft sediment rip-up clasts in loose sandy mud (cf. Hillenbrand et al., 2013). These deposits are differentiated from the subglacial till by their typically lower shear strengths (<40 kPa) and higher water content (Fig. 5). Loose diamicton overlying an iceberg-rafted deposit in core 10-44 is also interpreted as reworked by local iceberg turbation or possibly mass wasting on the flank of a Slyne Trough Moraine based on its lithologic similarity to the underlying sediment, abruptly lower shear strength and increasing sand content (cf. Vorren et al., 1983; Dowdeswell et al., 1994; Fig. 5). Iceberg turbate formation in the Slyne Trough is supported by previous micropalaeontological and geomorphic research that documents an increase in foraminiferal

test damage and intense iceberg scouring in the interval we interpret as reworked (Peters et al., 2015). An anomalously young radiocarbon age (15,876 Cal BP) from this reworked interval in core 10-44 is comparable to other chronologic inconsistencies in iceberg turbates (e.g. Hillenbrand et al., 2010) and suggests that on-ridge reworking occurred <16,000 yr BP.

4.2.3. Lithofacies association 3 (glacial to postglacial transition)

Lithofacies association 3 consists of four lithofacies (Dcm, GO, SH and GSH) deposited between the overlying sandy lithofacies of LFA 4 and the underlying glacial sediments of LFAs 2 and 1. Clasts within the Dcm diamictons and GO gravel are lithologically similar to those in the underlying deposits, suggesting a similar sediment source. Therefore the reduction in matrix material in LFA 3 suggests either increased rates of IRD production (cf. Kilfeather et al., 2011) or sediment winnowing (Eyles, 1988). The Dcm diamicton from the western Slyne Trough (cores 10-42, 10-44 and 10-45, Fig. 2a) that overlies the sub-ice shelf sediment has previously been interpreted as intense IRD rain-out sediment that records ice shelf breakup and subsequent current winnowing (Peters et al., 2015).

The SH and GSH lithofacies are composed largely or entirely of upward-fining bivalve shells and fragments within very small amounts of sand matrix, suggesting fine sediment winnowing in a biologically active palaeoenvironment (Flemming et al., 1992). The shell-rich deposits are interpreted to record sea level transgression based on their sharp lower contacts, upward fining and winnowed fines (cf. Chang et al., 2006). The shell hash of core 14-53 contains an 8-cm thick unit of massive, shell-rich sand (Fig. 5) that we interpret to likely record a period of relative, local palaeocurrent quiescence.

4.2.4. Lithofacies association 4 (postglacial deposition/reworking)

This LFA consists of Sh, Suf and Sm lithofacies. The poorly-sorted, yellowish sand at the top of all cores except core 14-59 (Fig. 5) is interpreted as postglacially reworked sediment based on its low mud content, low shear strength, typically low wet bulk density and high water content (cf.

Hillenbrand et al., 2013). Upward fining sand at or near the top of cores 10-35, 10-40, 10-42, 10-44 and 10-45 (Fig. 5) indicate reworking by gradually weakening bottom currents (Bishop and Jones, 1979; Fyfe et al., 1993; Viana et al. 1998), which is in accord with interpretations of winnowing in the underlying transitional sediments of LFA 3. Previous micropaleontological research on the Porcupine Bank is also compatible with an interpretation of winnowing and reworking by bottom currents (Smeulders et al., 2014; Peters et al., 2015). This upwards waning in palaeocurrent activity is interpreted as a record of postglacial sea level transgression across the continental shelf (cf. Amorosi et al., 1999; Barrie and Conway, 2002).

4.3. Core correlation and regional stratigraphy

Core correlations are based on LFA interpretations and from this four stratigraphic transects are produced that extend from west to east across the study area (Fig. 6). These transects cross all of the major glacigenic landforms in the study area and reveal glacial and postglacial depositional trends west of Ireland. The stratigraphic sequence is generally consistent between the cores and shows the following vertical stratigraphic sequence: subglacial traction till which shows a progressive decrease in shear strength upwards, glaciotectonite, glaciomarine deposits (plumite and iceberg-rafted sediment), a transgressive lag and current-reworked sand (Fig. 6). However, the following lateral patterns in sediment distribution across the shelf are also identified: (1) a general eastward (landward) increase in glaciotectonite, (2) a prevalence of reworked sediment near the GLGZW, (3) a general eastward thickening of the transitional, transgressive deposits (LFA 3), and (4) an occasional, marked thickening of the glaciomarine and postglacial deposits to the east of large moraines (e.g. cores 10-40, 10-45, 14-59, Fig. 6).

The ~2-4 m thick sedimentary record of the western Irish continental shelf is dominated by the glacigenic deposits of LFA 1 (Fig. 6). Subglacial traction tills are common at the base of the Midlandian glacial sedimentary record west of Ireland and their occurrence confirms previous research documenting grounded BIIS extension across the continental shelf (e.g. Ó Cofaigh et al., 2010; Peters et al., 2015). A less-compact till with a diffuse lower contact often overlies the

lowermost stiff basal till in cores from the shelf. This relatively soft till records increased pore water pressures that may have been caused by the underlying clay-rich, and thus lower porosity, stiff till which would have acted to impede pore water expulsion from the soft till (Fischer et al., 1999; Lian and Hicock, 2000; J. Evans et al., 2006). In places the tills are covered by glaciotectonite up to ≥1 m thick (Fig. 6). This glaciotectonite is most common towards the east of the study area (i.e. landward) and frequently occurs on the flanks of the Galway Lobe Moraine (Fig. 6).

A glaciomarine deposit with a diffuse lower contact overlies the till and glacitectonite in all cores except 10-38 (Fig. 6). It is interpreted as a product of suspension settling from meltwater plumes during BIIS retreat. It ranges in thickness from 12-224 cm thick with a mean thickness of ~75 cm. The thickest glaciomarine deposits are massive, muddy, IRD-rich diamictons; these deposits are >100 cm in the Slyne Trough (Cores 10-44 and 10-45) and just east of the Connemara Lobe Moraine (core 10-40, Fig. 6). These areas of thick glaciomarine deposition are interpreted as a record of either prolonged sub-ice shelf (cf. Kilfeather et al., 2011) or iceberg rafted sedimentation. The lack of glaciomarine sediment in core 10-38 is interpreted as an erosional unconformity caused by current winnowing, possibly facilitated by the bathymetric high formed by the Connemara Lobe Moraine (Figs. 2a, 3a).

Areas of remobilised glaciomarine sediment overly the plumite near moraines (cores 10-44, 14-42, 14-54 and 14-57) and, less frequently, on the inner shelf (core 14-41) (Fig. 6). Most of these reworked deposits likely record iceberg turbation on or near moraine ridges. This interpretation is consistent with a previous examination of iceberg plough mark geomorphology in the Slyne Trough, which documents iceberg grounding against moraine ridges and a roughly northward palaeocurrent (Peters et al., 2015). Postglacial mass wasting, which likely would have been most intense on the morainic ridges, is another potential source for sediment reworking (cf. McCabe, 1986).

A unit of shell-bearing, bottom-current-winnowed sediment interpreted to record a transitional period from glacial to postglacial conditions overlies the glaciomarine deposits in each core except

core 10-36 (Fig. 6). These transitional sediments range in thickness from 6-146 cm (cores 10-35 and 14-59, respectively) and are thickest to the east (Fig. 6). This sediment also typically contains progressively more biogenic material towards the east (Fig. 6). The thickest (up to 21 cm) of the lithic-dominated, winnowed sediment units are found in the Slyne Trough; this is interpreted as a result of coarse sub-ice shelf or ice-proximal sediment supply that led to increased IRD production after ice shelf break up. The relative abundance of large lithic clasts was likely increased by winnowing from a northward Slyne Trough palaeocurrent that developed following ice shelf break up (Peters et al., 2015). Another thick, lithic, winnowed sediment unit overlies the highly-consolidated, subglacial till at the base of core 10-38 (Figs. 5, 6). This area (the crest of the Connemara Lobe Moraine, Figs. 2a, 3a) is interpreted to have experienced particularly high amounts of winnowing based on a lack of preserved glaciomarine sediment in core 10-38, the thickness of the winnowed transitional unit (20 cm), and the general absence of fine-grained sediment in the GO facies (Fig. 5). The eastern, shell-dominated, winnowed sediment is thickest within 50 km of shore (cores 10-40 and 14-59, Fig. 2a) where it is largely composed of biogenic material (Figs. 5, 6). The eastern thickening of the unit and increasing shell content is consistent with reworking during sea-level transgression (e.g. Saito et al., 1998), thus, we refer to these deposits collectively as a transgressional lag (cf. Chang et al., 2006).

Mean magnetic susceptibility values show a distinct eastward (i.e. shoreward) increase (Fig. 6). Values for cores >40 km west of the GLGZW and Connemara Lobe Moraine (cores 10-35, 10-36, 10-42, 10-44, 10-45; Fig. 2a) range from 11-36 10^{-8} SI (Figs. 5, 6) with an average of 19.75 10^{-8} SI. Conversely, the magnetic susceptibility of cores from near to or east of these large moraines (Fig. 2a) ranges from 21-135 10^{-8} SI (Figs. 5, 6) with a mean of 83.86 10^{-8} SI. This discrepancy is interpreted as the signature of increasing amounts of glacially-mobilised terrigenous sediment supply to the shelf (Robinson et al., 1995; Shevenell et al., 1996). This interpretation is supported by previous sedimentary interpretations in the Slyne Trough and Porcupine Bank (Peters et al., 2015).

Elphidium clavatum was found to be the dominant benthic foraminifera below LFA 3 in most of the micropalaeontologically-examined cores, usually near the contact with the overlying transgressional lag (Figs. 5, 6). The dominance of *E. clavatum* typically diminishes upwards in cores from the shelf (Fig. 5). This *E. clavatum* range indicates a palaeoenvironment with variable salinity, high sedimentation rates, cold (<1ºC) average sea temperatures, and potential sea ice cover (Mudie et al., 1984; Hald and Korsun, 1997; Polyak et al., 2002; Stalder et al., 2014). This inferred micropaleontological environment supports our sedimentological interpretation of glaciomarine deposition from meltwater and iceberg rafting with possible areas of seasonal sea ice cover. The bottom of the rain-out sediment in core 14-36 and the top of the subglacial sediment in cores 10-38, 14-41 and 14-57 are devoid of any foraminiferal tests (Fig. 6), indicating a depositional environment dominated by terrigenous sediment supply where little or no pre-glacial marine sediment was incorporated into the till (cf. Ó Cofaigh et al., 2011; McCabe and Clark, 2003).

5. Discussion

5.1. LGM ice sheet extent, configuration and chronology on the shelf west of Ireland

The moraines on the Porcupine Bank and Slyne Trough (Peters et al., 2015) and the large, arcuate WIM (Fig. 2) provide geomorphic evidence for an extensive grounded BIIS on the shelf west of Ireland. This geomorphic interpretation is also supported by the presence of subglacial traction tills in cores from the shelf (Fig. 6). These moraines appear to be restricted to less than ~350 mbsl (Fig. 2) and are oriented roughly parallel to the shelf break, suggesting that at maximum extent the BIIS consisted of a grounded ice mass that was calving into deep water (cf. Sejrup et al., 2005); this large ice mass was likely fed by ice draining from counties Mayo, Galway, Clare and Kerry, Ireland (Greenwood and Clark, 2009; Fig. 2a). Based on the geomorphic and sedimentary evidence documented in this study, the ice sheet at its maximum extended to within ~20 km of the shelf break. This is compatible with previous geomorphic reconstructions and conceptual models of the western BIIS (e.g. Sejrup et al., 2005; Greenwood and Clark, 2009).

694 The presence of overconsolidated subglacial traction tills with low water content at the base of
695 the sedimentary sequence across the shelf west of Ireland (Fig. 6) suggests that initial BIIS advance
696 was extensive and may have occurred largely without ice streaming (cf. Wellner et al., 2001; Shipp et
697 al., 2002; Dowdeswell et al., 2004; Evans et al., 2005; Ó Cofaigh et al., 2005, 2007). This
698 interpretation is also consistent with delayed IRD sedimentation on the Porcupine Bank in relation to
699 the Rosemary Bank (Scourse et al., 2009).

700 The till blanket that covers the continental shelf (Fig. 6) is dated to ≤24,067 Cal BP (Table 2) in
701 the Slyne Trough, within 50 km of the shelf break (cf. Peters et al., 2015, Fig. 2a). This is compatible
702 with other radiocarbon ages that constrain initial advance of Irish Sea ice in the Celtic Sea (Fig. 1) to
703 ≤24,000 Cal BP (Ó Cofaigh and Evans, 2007; Ó Cofaigh et al., 2012). An AMS radiocarbon age
704 from the glaciomarine sediment that drapes the WIM (Figs. 6, 7) constrains the timing of ice-
705 proximal, deglacial deposition to 20,944 Cal BP (core 10-35, Table 2). This age indicates that the
706 WIM is blanketed by glaciomarine sediment from Midlandian deglaciation and its stratigraphic
707 relationship to the underlying subglacial till suggests in turn that the WIM was deposited by the last
708 BIIS during MIS 2. The 20,944 Cal BP age is ~900 years younger than glaciomarine sedimentation in
709 the Slyne Trough (21,841 Cal BP, core 10-45, Table 2); this suggests that initial ice retreat may have
710 started over the bathymetrically deep Slyne Trough.

711 ***5.2. Ice shelf chronology and BIIS dynamics during GLGZW formation***

712 Sedimentological and micropalaeontological evidence in the Slyne Trough (Peters et al., 2015)
713 indicate local BIIS uncoupling and ice shelf formation by 21,841 Cal BP (core 10-45, Table 2, Figs. 6,
714 7). Ice shelf formation precedes the rapid sea-level rise recorded at Kilkeel Steps (Clark et al., 2004;
715 Fig. 1) by ~2,800 years and follows the Greenland Interstadial 2 warming event (~21,000 Cal BP)
716 recorded by the GRIP ice core $\delta^{18}O$ record (Dansgaard et al., 1993; Björck et al., 1998) by <200 years.
717 This chronologic sequence suggests that initial BIIS thinning over the Slyne Trough may have been
718 the result of climate amelioration or variations in Atlantic Meridional Overturning Circulation (cf.
719 Clark et al., 2012b).

720 The presence of the GLGZW indicates that the ice sheet underwent a still-stand on the mid-
721 shelf following initial recession from the WIM. This must have occurred after the formation of an ice
722 shelf over the Slyne Trough at 21,841 Cal BP, core 10-45, Table 2; Peters et al., 2015) and prior to the
723 biomineralization of foraminiferal tests found in core 14-54 (21,161 Cal BP, Figs. 6, 7). This means
724 that the grounding zone retreated eastward across ~50 km of seafloor over a period of ~680 years at a
725 rate of ~74 m/yr. This ~50 km section of seafloor is devoid of any morainic ridges, suggesting that
726 grounding zone retreat back to the mid-shelf and the position of the GLGZW was probably
727 continuous and un-interrupted by stillstands or readvances (Dowdeswell et al., 2008). Comparable
728 retreat rates are recorded for modern marine-terminating outlet glaciers on the Antarctic Peninsula
729 (Cook et al., 2005) and similar episodic retreat has been proposed for other areas of the western BIIS
730 marine margin (Bradwell et al., 2008; Ó Cofaigh et al., 2010).

731 The arcuate shape of the GLGZW closely mimics the orientation of the 200-m isobath (Fig.
732 2a), suggesting that grounding zone stabilization was controlled largely by bathymetry (cf. Ship et al.,
733 1999). Thus, the GLGZW likely records a period of BIIS reconfiguration and stabilisation along the
734 shallower, mid continental shelf. This reconfiguration likely resulted from increased ice buoyancy on
735 the outer shelf (i.e. areas of modern depths >200 m, Fig. 2a), either from sea level rise (Eyles and
736 McCabe, 1988, McCabe et al., 2005) or ice thinning caused by AMOC variations (Clark et al.,
737 2012b). The composite shape of the GLGZW, with at least two distinct flat-topped ridges (Fig. 3ii,
738 iii), most likely records minor oscillations of the grounding zone. Specifically, the westernmost flat-
739 topped ridge likely records a period of grounding-zone wedge deposition below a thicker ice shelf that
740 created a smaller vertical accommodation space (Batchelor and Dowdeswell, 2015). Further evidence
741 of a dynamic grounding zone is provided by glaciotectonised plumite deposits near the flanks of the
742 GLGZW. That this glaciotectonism occurred without the formation of distinct ice-terminal landforms
743 indicates periods of minor readvance or recoupling along the grounding zone.

744 Extensive iceberg scouring west of the GLGZW indicates that the ice shelf that flanked the
745 western BIIS marine margin retreated via calving. This interpretation is consistent with geomorphic

746 investigations on the shelf west of Donegal Bay, north of the study area (Fig. 1). There, extensive
747 zones of iceberg scouring are interpreted to record rapid ice loss by calving following BIIS maximum
748 extension to the shelf break (Benetti et al., 2010; Dunlop et al., 2010; Ó Cofaigh et al., 2010). A
749 period of increased iceberg production following ice shelf formation is also evidenced by the massive
750 clast-rich diamicton commonly overlying till on the continental shelf (Fig. 6). Radiocarbon dates
751 from the iceberg-rafted deposits in cores 10-35 on the WIM and 10-45 in the Slyne Trough restrict
752 this phase of calving retreat to ≲21,000 Cal BP (Table 2, Fig. 6), which is roughly coincident with
753 post- Heinrich Event 2 peaks in BIIS-IRD production in cores from the Porcupine Seabight and
754 Rockall Trough (Peck et al., 2006; Scourse et al., 2009). The ice shelf disintegrated, or at least its
755 terminus retreated to a point on the continental shelf east of the GLGZW by ≤18,517 Cal BP, when
756 foraminiferal tests were biomineralized in core 14-53 (Table 2). This allows an estimate for ice shelf
757 duration of ≲2,500 years and a minimum rate of ice shelf retreat over the ~60-km long expanse
758 between the Slyne Trough and the GLGZW, to be calculated at ~24 m/yr. However, it is likely that
759 this retreat was not steady state and that rapid sea-level rise occurring ~19,000 Cal BP (Clark et al.,
760 2004) may have exacerbated the calving rate of this ice margin.

761 Grounding-zone wedges with similar dimensions to the GLGZW that occupy other glaciated
762 continental shelves offshore of Antarctica and Norway (e.g. Shipp et al., 2002; Ottesen et al., 2005)
763 are associated with stillstands during episodic ice retreat (Howat and Domack, 2003; Dowdeswell et
764 al., 2008). Although no sediment flux rate can yet be calculated for the GLGZW, grounding-zone
765 wedges with comparable dimensions have typically been shown to record stillstands that lasted
766 decades or centuries (Batchelor and Dowdeswell, 2015, and references therein). Thus, it is likely that
767 the GLGZW formed along a grounding zone that was stable for a relatively long time while its
768 vertical accretion was constrained by a large, buttressing ice shelf. It is evident that the stillstand
769 marked by the GLGZW occurred after the deposition of till in the Slyne Trough dated to ~24,067 Cal
770 BP (Peters et al., 2015; Table 2, Figs. 6, 7) and prior to the formation of the nearby Galway Lobe
771 Readvance Moraine <18,517 Cal BP (core 14-53, Table 2, Figs. 5, 6, 7). This ~5,500 year period
772 represents the maximum duration of grounding-zone proximal deposition along the GLGZW.

However, it is more likely that the GLGZW was deposited over a period of <3,300 years, defined by the age of ice-shelf inception over the Slyne Trough (21,841 Cal BP) and the age of foraminiferal tests within glacitectonised sediment to the east (18,517 Cal BP).

5.3. BIIS dynamics and chronology following ice shelf break up

A glacitectonised plumite in core 14-53 (Figs. 5, 6) contains calcareous benthic foraminifera that provide an AMS radiocarbon date of 18,517 Cal BP (Table 2). The date provides a maximum age for the glaciotectonisation. This date is approximately 2,700 years older than previous estimates of the timing of deglaciation from surface exposure dating from the west coast of Ireland, which was calculated to ~15.85 ka BP from four cosmogenic ages (Table 3) (Bowen et al., 2002; Ballantyne et al., 2008). Collectively these dates constrain the formation of the Galway Lobe Readvance Moraine to a ~2,700 year window from ≤18,400 Cal BP to >15.85 ka BP (Fig. 7). Radiocarbon ages on ice sheet readvance(s) in eastern Ireland during the Clogher Head Stadial (<18,200-17,100 Cal BP, McCabe et al., 2007; Clark et al., 2012b) and cosmogenic ages interpreted to constrain the age of readvances in western Ireland during the Killard Point Stadial (Table 3; ≥17.1-≥16.0 ka BP, Clark et al., 2012b) fall within the range of age constraints for this readvance on the Irish continental shelf (Fig. 7). This suggests that climactic forcing during those stadials may have influenced BIIS readvance(s) offshore of western Ireland; however, based on our existing chronology the role of internal glaciodynamic forcing mechanisms (e.g. changes in subglacial bed conditions) cannot be ruled out.

The duration of ice occupation at the Galway Lobe Readvance Moraine is unknown, but the mean post-LGM deglaciation age for the west coast of Ireland (~15.85 ka BP, Table 3) indicates that the BIIS retreated from this position across ~130 km of continental shelf to the shore of County Clare (Figs. 2a, 7) at a minimum rate of ~48 m/yr—calculated assuming moraine formation at the time of age-constraining biomineralization (18,517 Cal BP). If the Galway Ice Lobe retreated following a Killard Point readvance at ~17,000 Cal BP, this would provide a retreat rate of ~113 m/yr.

798 The general southward progression of the maximum extent of the three largest ice marginal
799 features (WIM, GLGZW and Galway Lobe Readvance Moraine) indicates a possible increase in
800 topographic constraint (likely from the Maumturk Mountains, Fig. 2a) on ice dynamics imposed on
801 the thinning, retreat-phase BIIS (cf. Bradwell et al., 2008; Greenwood and Clark, 2009; Clark et al.,
802 2012a). Unlike the three largest ice-terminal landforms in the study area, the Connemara Lobe and
803 Mayo Lobe moraines have an arcuate shape that is unrelated to local bathymetry and suggestive of
804 outflow from local, terrestrial source areas (Fig. 2a). These lobate moraines likely record the
805 development of topographically-restricted ice-flow outlets on the west of Ireland that developed
806 following BIIS thinning (cf. Bradwell et al., 2008). The moraines are well preserved, truncate the
807 GLGZW and are situated roughly within the radius of the WIM (Figs. 2a, 7), suggesting that these
808 smaller moraines record BIIS readvances during overall retreat. These readvances identify the
809 evolution of deglacial ice drainage regimes west of Ireland (cf. Greenwood and Clark, 2008). The
810 Connemara Lobe Moraine is at least partially composed of soft, probably dilatant, subglacial till
811 overlain in areas by glaciotectonised glaciomarine sediment (cores 10-40 and 14-59; Fig. 6). The
812 dilatant till suggests periods of accelerated ice flow or ice streaming over bed material with high pore
813 water pressures (Ó Cofaigh and Evans, 2001; Ó Cofaigh et al., 2007). The till sampled in core 14-59
814 incorporates calcareous marine biogenic material that provides an age for the deposition of the top
815 four metres of the Connemara Lobe Moraine of ≤15,148 Cal BP (Table 2; Fig. 7). This suggests that
816 the Connemara Lobe advanced to this point on the continental shelf by ~15,000 Cal BP.
817 Alternatively, the moderately stiff (~40 kPa) diamicton at the base of core 14-59 could have been
818 formed by iceberg turbation or debris flows; however the high density, low water content and folding
819 of this deposit (Fig. 5) are more compatible with and interpretation of subglacial till. This indicates
820 that the western BIIS had a marine margin 1,000 years after the Killard Point Stadial. We suggest that
821 internal (glaciodynamic) forcing mechanism(s) are most likely to have triggered this readvance.
822 However, we cannot rule out the possibility that readvance was climatically-driven and associated
823 with the Nahanagan Stadial (Younger Dryas) although this would imply significantly more extensive
824 glacier growth during this period in western Ireland than has hitherto been proposed.

825 Although no direct age constraints are available for the Mayo Lobe Moraine, it was likely
826 deposited after the formation of the GLGZW at 21,841-18,517 Cal BP. An estimated age of
827 deposition of <21,000 Cal BP for the Mayo Lobe Moraine is ~5,400 years older than the cosmogenic
828 ages that define the Killard Point Readvance at Furnace Lough (Clark et al., 2009b; Table 3). Thus,
829 the Mayo Lobe Moraine is interpreted as pre-dating the Killard Point Stadial.

830 The readvances identified here on the basis of the core sedimentology and associated
831 geochronology post-date break-up of the ice-shelf farther offshore in the Slyne Trough (Peters et al.,
832 2015, Fig. 7). This suggests that the loss of the buttressing, floating ice mass could have initiated a
833 period of accelerated westward flow similar to that which has been observed for ice sheet outlets
834 around the Antarctic Peninsula (cf. Scambos et al., 2004).

835

836 Table 3: Referenced, cosmogenic nuclide ages from near the coast of counties Mayo, Galway and Clare, Ireland.

Age (ka)	Avg. age (ka)*	Isotope	Location (abbreviation)*	Elevation (m asl)	Interpretation	Reference (age)	Reference (interpretation)
14.5±0.9	13.73	^{10}Be	Lough Acorrymore (LA)	287	Nahanagan readvance age constraint	Ballantyne et al. (2008)	Ballantyne et al. (2008)
11.7±0.7		^{10}Be		190			
15.0±1.0		^{10}Be		198			
15.1±1.0	14.15	^{10}Be	Mweelrea (MW)	305	Post-LGM deglaciation age constraint	Ballantyne et al. (2008)	Ballantyne et al. (2008)
13.2±0.8		^{10}Be		650			
15.3±1.0	--	^{36}Cl	Kilkee (KE)	66	Post-LGM deglaciation age constraint	Bowen et al. (2002)	Bowen et al. (2002)
15.7±1.0 15.2±1.0 14.3±0.9 17.3±1.0 16.4±1.1 16.1±0.7 15.4±0.9 14.1±0.7	15.6±0.4	^{10}Be	Furnace Lough (FL)	14-74	Killard Point readvance age constraint	Clark et al. (2009b)	Clark et al. (2009b)

16.7±1.0	--	^{10}Be	Farnaght Hill (FH)	125	Post-LGM deglaciation age constraint	Ballantyne et al. (2008)	Ballantyne et al. (2008)
16.4±1.9 17.5±3.7	16.95	^{36}Cl ^{36}Cl	Lough Nakeeroge (LN)	5 5	Killard Point readvance age constraint	Bowen et al. (2002)	Ballantyne et al. (2008)
17.1±1.1 17.2±1.1	17.15	^{10}Be ^{10}Be	Anaffrin East Col (AC)	440 440	Post-LGM deglaciation age constraint	Ballantyne et al. (2008)	Ballantyne et al. (2008)

* Used in Fig. 7.

6. Conclusions

- The ~80-km long, arcuate West Ireland Moraine reaches to within 20 km of the shelf break west of Ireland and records the minimum westward, grounded extension of the BIIS ≤24,067 Cal BP. This moraine is constructed, at least in part, from subglacial till and is capped by glaciomarine sediment that was deposited ~2,100 Cal BP. This age constraint supports an interpretation of corrugation genesis from the periodic grounding of an overriding ice shelf that extended over the Slyne Trough.

- Overconsolidated subglacial till common at the base of the stratigraphic sequence across the continental shelf indicates that the BIIS advanced to its maximum offshore position without streaming or surging. However, after the initiation of retreat across the continental shelf west of Ireland (≤21,841 Cal BP), the BIIS likely experienced accelerated flow over a dilatant till with increased pore water pressures. These periods of accelerated flow formed readvance moraines.

- An ice shelf formed over the Slyne Trough and extended over the West Ireland Moraine following the advance of grounded ice ≤24,067 Cal BP. AMS radiocarbon dated sub-ice shelf deposits indicate that this ice shelf formed ≤21,841 Cal BP over the Slyne Trough and within ~800 years of the Greenland Interstadial 2 warming event (~21,000 BP), suggesting

856 that the westernmost BIIS may have uncoupled and formed a floating ice shelf after thinning
857 that was induced by variations in the Atlantic Meridional Overturning Circulation. Two AMS
858 radiocarbon dates from ice-proximal, IRD-rich glaciomarine sediment constrain the calving-
859 dominated, eastward retreat of this ice shelf to have begun by approximately <21,000 Cal BP.

860 • The BIIS grounding zone retreated during a single event, without forming moraines or
861 grounding-zone wedges, across ~50 km of seafloor. This retreat likely took place over a
862 period of ~680 years at a rate of ~74 m/yr. The grounding zone stabilised near and parallel to
863 the 200-m isobath, suggesting a bathymetric control on its retreat.

864 • The bathymetrically-controlled grounding zone most likely persisted in roughly the same
865 location for a maximum of <3,300 years. Whilst in this position, the flanking ice shelf
866 buttressed ice flow and added to the stability of the retreat stillstand. During this stillstand,
867 subglacial sediment delivery along the grounding zone resulted in the formation of a large
868 (~150-km long, up to 22-km wide, and up to 20-m thick) grounding-zone wedge. This
869 grounding-zone wedge is termed the Galway Lobe grounding-zone wedge (GLGZW) because
870 it is interpreted to have formed against ice draining from Galway Bay, Ireland (the Galway
871 Lobe).

872 • During the stillstand that formed the GLGZW, the position of the grounding zone on the shelf
873 was relatively stable, but several minor fluctuations in ice dynamics formed the GLGZW as a
874 composite landform. Glaciotectonised glaciomarine deposits are common on the flanks of the
875 GLGZW, and record periods of local ice recoupling or readvance, one of which is dated to
876 21,161 Cal BP. Retreat from the GLGZW was complete by <18,517 Cal BP.

877 • BIIS marine margin retreat was characterised by a topographically-driven modification of ice
878 flow dynamics probably associated with overall ice sheet thinning. This increased
879 topographic influence on the retreating BIIS is evidenced by migrating positions of moraines
880 and a general eastwards decrease in moraine size. These landform characteristics record the

881 increasingly lobate structure of the BIIS during retreat, which is likely the signature of ice
882 sheet thinning.

883 • The Galway Lobe Readvance Moraine was formed following grounding zone retreat <18,517
884 Cal BP. Although no direct age constraints are available, the smaller Mayo Lobe Moraine
885 was likely deposited after the formation of the Galway Lobe Readvance Moraine and is at
886 least younger than the 21,841-18,517 Cal BP GLGZW. The Connemara Lobe moraine was
887 formed by an ice lobe that advanced onto the continental shelf after the formation of the
888 GLGZW, likely <15,148 Cal BP and truncated surrounding morainic landforms. This
889 indicates that the ice sheet underwent readvances on the shelf during deglaciation although
890 our existing chronology does not yet allow us to determine conclusively if these readvances
891 were glaciologically (internally) driven or a response to climatic forcing.

892 • Estimated rates of BIIS retreat vary drastically. Following ice shelf formation over the Slyne
893 Trough, the BIIS's grounding zone retreated at a rate of ~74 km/yr before stabilizing and
894 depositing the GLGZW. The ice shelf terminus retreated from the Porcupine Bank to the
895 GLGZW at a minimum rate of ~24 m/yr before the grounding zone withdrew from the
896 stillstand marked by the GLGZW. Following GLGZW deposition, BIIS marine margin
897 retreat was punctuated by at least one readvance. During this continued retreat the marine-
898 terminating ice sheet comprised of several discreet lobes, the largest of which formed the
899 Galway Lobe Readvance Moraine prior to retreating ~130 km to the west coast of Ireland at a
900 likely rate of ~113 m/yr. This highlights a drastic increase in marine margin retreat following
901 the loss of the ~50-km wide ice shelf.

902 ## 7. Acknowledgements

903 JLP acknowledges a University of Ulster PhD studentship and Vice-Chancellor's Scholarship
904 from 2013-2016. This work was supported by the NERC Radiocarbon Facility NRCF010001
905 (allocation number 1722.0613), NERC consortium grant NE/J009768/1, for radiocarbon dating.

Further radiocarbon dating support was provided by the International Association of Sedimentologists (Postgraduate Research Grant, 1st session, 2014) and the Raidió Teilifís Éireann (RTE) broadcasting company for the television programme 'The Investigators'. Thanks to Derek Fabel at the Scottish Universities Environmental Research Centre, University of Glasgow, for his help during radiocarbon calibrations. Grateful thanks to Christian Wilson of Ocean DTM for Olex data-acquisition support, Robin Edwards at Trinity College, Dublin for the use of his MALVERN Mastersizer© for grain size analyses and sample processing, and Stephen McCarron at the National University of Ireland, Maynooth for the use of the GEOTEK multi-sensor core logger. We would like to thank the Captain and Crew of the RV *Celtic Explorer*, cruise participants and Mr Áodhan Fitzgerald of the Marine Institute, for their invaluable assistance during cruises CE10008 and CE14004 (WICPro). The research surveys were carried out under the Sea Change strategy with the support of the Marine Institute and the Marine Research Sub-programme of the National Development Plan 2007–2013.

Figure Captions

Fig. 1: Regional map locating the study area (shown in Fig. 2) and core locations amongst prominent glacial landforms, ice streams and the last BIIS's maximum extent (Sejrup et al., 2005; Scourse et al., 2009; Clark et al., 2012a; Peters et al., 2015). The 'Previously accepted Killard Point ice limit' is compiled from reconstructions by McCabe et al. (1998) in Ireland and the theoretical model of BIIS extent at approximately the 17 ka BP isochrone synthesised by Clark et al. (2012a).

Fig. 2: (a) Study area map showing the Olex bathymetric dataset used for the geomorphic analyses and core locations relative to modern land. The topographic DEM (NASA, Shuttle Radar Topography Mission) reveals regional, bedrock-controlled trends in geomorphology. The labelled transects delineate the seafloor profiles shown in Fig. 3. Isobaths are shown every 100 mbsl and created from Irish National Seafloor Survey (INSS, www.infomar.ie) data and the United Kingdom Hydrographic Office (UKHO; www.ukho.gov.uk) data. Yellow arrows delineate the western edge of the low, flat-topped ridge (Fig. 3ii); red arrows delineate the western edge of the large flat-topped ridge (Fig. 3iii); black dotted lines delineate the eastern edge of the smaller, nested arcuate ridge. (b-e) Classified (20-m) hillshaded Olex data showing: (b) detail of the Slyne Trough Moraines and the corrugated southern section of the larger arcuate ridge on the outer shelf; the arrow marks an area of intense iceberg scouring and lodgement and dashed, white line highlights the geographic relationship between the moraines and corrugations (Peters et al., 2015); (c) detail of a large seafloor furrow with a corrugated base, gradual, progressively-deepening southern terminus and abrupt, pit-like northern terminus (marked by arrow); the white 'X' highlights noise in the Olex data that manifests horizontally across the data; (d) sketch of furrows and pits in (c). Abbreviations: WIM = West Ireland Moraine, GLGZW = Galway Lobe Grounding Zone Wedge, GLRM = Galway Lobe Readvance Moraine, BB = Blacksod Bay, CB = Clew Bay, KB = Killary Bay, GB = Galway Bay, SRE = Shannon River Estuary.

Fig. 3: Seafloor profiles characterising the glacial landforms in the study area. Bold grey lines labelled i, ii and iii delineate the western flanks of seafloor ridges that extend between profiles but do not represent ridge geography (Fig. 2a). (a) Profile X-X' reveals the northern extension of the low-relief, flat-topped ridge (ii) that flanks the largest arcuate ridge in the study area (Fig. 2a) and the steep-sided arcuate ridge that truncates the large ridge. The location of core 10-40 is shown. (b) Profile W-W' shows the northern extent of the westernmost arcuate ridge (WIM, i), the complex of large, flat-topped, arcuate ridges (ii and iii) and the ridge-free, furrowed seafloor in between. The location of cores 10-35, 10-36 and 14-53 are shown. (c) Profile Y-Y' exposes the corrugated southern extent of the westernmost arcuate ridge (i), the complex of large, flat-topped, arcuate ridges (ii and iii) and the ridge-free, furrowed seafloor in between. The location of core 14-54 is shown.

(d) Profile Z-Z' depicts the deep furrows with flanking berms that are abundant in the Slyne Trough and the poorly-defined southern extent of the complex of large, flat-topped arcuate ridges. The location of core 14-36 is shown.

Fig. 4: Representative x-radiograph facies. (a) X-radiograph and structure sketch of in Dmm_c from core 10-38 exposing a ~40° preferential clast alignment and showing the location of a shear stress measurement of 80 kPa. (b) X-radiograph, structure sketch and photograph of deformed Fl from core 14-59 revealing apparent clast alignment to strain and showing the location of a shear stress measurement of 28 kPa. (c) Dmm from core 10-40 exposing rhythmic areas of high clast concentration. (d) Clast-rich Fl(s) from core 14-57 exposing a prominent shear plane (top = white arrow, bottom = black arrow) with a large (~3-cm long) clast (arrow labelled 'c') aligned in the direction of shear. (e) Fl(s) from core 14-41; well-defined laminae reveal a ~40° reverse fault with an offset of ~2 cm (top of offset = white arrow, bottom of offset = black arrow). (f) Dcm with a diffuse lower contact overlying Dmm in core 14-59; black arrow marks an area devoid of large clasts but filled with interstitial sandy matrix. (g) Dms from core 10-35 exposing clast-rich, horizontal stratification; black arrows mark contacts between select strata. (h) GO from core 10-38; black arrow marks an area of void space between clasts. (i) Diffuse contact between Sm and underlying SH in core 14-54; large shells are exposed as light-grey curvilinear shapes. (j) Diffuse contact between Sm and underlying Suf in core 10-35; white dashed line marks the location of the GSA analyses that yielded 0.3% >1 mm lithic fragments; GSA analysis that yielded 16% >1 mm lithic fragments was taken at the bottom of the core section shown; white arrow marks an area of relatively low-density, poorly-sorted, shell-fragment-rich material interpreted as an infilled burrow (bioturbation); shell fragments are exposed as light-grey/white.

Fig. 5: Plots of core data from the western Irish continental shelf. From left: true-colour photograph, sketch of prominent structures discerned by x-radiograph analyses, log of lithology and sedimentary structures, lithofacies abbreviations and extents of LFAs, grain size data, sediment density (wet bulk) and (in cores 10-40 and 14-59) counts of lithic fragments >1 mm, sediment shear strength and water content (percent by weight), magnetic susceptibility and relative abundance of the benthic foraminifer *Elphidium excavatum* forma *clavatum*. AMS radiocarbon sample locations (m bsf) are marked by horizontal, dashed yellow lines; ages are provided in Cal BP and photographs of the dated materials are shown.

Fig. 6: Core correlations revealing continental shelf stratigraphy west of Ireland and exposing the glacial and postglacial depositional history associated with the last BIIS. Sediment core data is shown in detail in Fig. 5. Abbreviations: WIM = West Ireland Moraine; KLM = Killary Lobe Moraine; GLGZW = Galway Lobe Grounding-Zone Wedge; PBM = Porcupine Bank Moraine; STMs = Slyne Trough Moraines.

Fig. 7: Schematic map of study area showing isochrones derived from AMS radiocarbon data (Table 2) and analyses of geomorphology and stratigraphy that constrain the BIIS marine-terminating margin during retreat. AMS radiocarbon ages are displayed in coloured text that depicts the LFA that was sampled to provide the date; LFA 4 = postglacial reworking, LFA 2 = glaciomarine deposition, LFA 1 = advance-phase till or glacitectonite. Cosmogenic ages referred to in the text are shown with ages and abbreviations introduced in Table 3. Flowlines are generalised and determined geomorphically. The labelled blue arrow illustrates ice shelf retreat at a rate of ~24 m/yr and the labelled red arrows illustrate grounding line retreat at ~74 m/yr west of the Galway Lobe Grounding-Zone Wedge (GLGZW) and ~113 m/yr east of the GLGZW.

References

Amorosi, A., Colalongo, M., Pasini, G., Preti, D. (1999). Sedimentary response to Late Quaternary sea-level changes in the Romagna coastal plain (northern Italy). *Sedimentology*, 46(1), 99-121.

Andreassen, K., Winsborrow, M.C., Bjarnadóttir, L.R., Rüther, D.C. (2014). Ice stream retreat dynamics inferred from an assemblage of landforms in the northern Barents Sea. *Quaternary Science Reviews*, 92, 246-257.

988 Ballantyne, C.K., Stone, J.O., McCarroll, D. (2008). Dimensions and chronology of the last ice sheet
989 in Western Ireland. *Quaternary Science Reviews*, 27(3-4), 185-200.

990 Barrie, J.V., Conway, K.W. (2002). Rapid sea-level change and coastal evolution on the Pacific
991 margin of Canada. *Sedimentary Geology*, 150(1), 171-183.

992 Batchelor, C., Dowdeswell, J. (2015). Ice-sheet grounding-zone wedges (GZWs) on high-latitude
993 continental margins. *Marine Geology*, 363, 65-92.

994 Belderson, R.H., Kenyon, N.H., Wilson, J.B. (1973). Iceberg plough marks in the northeast Atlantic.
995 *Palaeogeography, Palaeoclimatology and Palaeoecology*. 13, 215–224.

996 Benetti, S., Dunlop, P., Ó Cofaigh, C. (2010). Glacial and glacially-related features on the continental
997 margin of northwest Ireland mapped from marine geophysical data. *Journal of Maps,* 6(1),
998 14-29.

999 Benn, D.I., Evans, D.J. (1996). The interpretation and classification of subglacially-deformed
1000 materials. *Quaternary Science Reviews*, 15(1), 23-52.

1001 Bennett, M.M., Glasser, N.F. (2011). *Glacial geology: ice sheets and landforms*, John Wiley & Sons.

1002 Bentley, M., Evans, D., Fogwill, C., Hansom, J., Sugden, D., Kubik, P. (2007). Glacial
1003 geomorphology and chronology of deglaciation, South Georgia, sub-Antarctic. *Quaternary*
1004 *Science Reviews*, 26(5), 644-677.

1005 Bentley, M.J., Fogwill, C.J., Le Brocq, A.M., Hubbard, A.L., Sugden, D.E., Dunai, T.J., Freeman,
1006 S.P. (2010). Deglacial history of the West Antarctic Ice Sheet in the Weddell Sea embayment:
1007 constraints on past ice volume change. *Geology*, 38(5), 411-414.

1008 Bishop, P., Jones, E.J.W. (1979). Patterns of glacial and post-glacial sedimentation in the Minches,
1009 North-West Scotland. *Elsevier Oceanography Series*, 24, 89-194.

1010 Björck, S., Walker, M.J., Cwynar, L.C., Johnsen, S., Knudsen, K.L., Lowe, J.J., Wohlfarth, B. (1998).
1011 An event stratigraphy for the Last Termination in the North Atlantic region based on the

1012 Greenland ice-core record: a proposal by the INTIMATE group. *Journal of Quaternary*
1013 *Science*, 13(4), 283-292.

1014 Blake, E., Clarke, G.K., Gérin, M.C. (1992). Tools for examining subglacial bed deformation. *Journal*
1015 *of Glaciology*, 38, 388-396.

1016 Bond, G.C., Showers, W., Elliot, M., Evans, M., Lotti, R., Hajdas, I., Bonani, G., Johnson, S. (1999).
1017 The North Atlantic's 1-2 Kyr Climate Rhythm: Relation to Heinrich Events,
1018 Dansgaard/Oeschger Cycles and the Little Ice Age. *Mechanisms of global climate change at*
1019 *millennial time scales*, pp.35-58.

1020 Boulton, G.S. (1986). Push-moraines and glacier-contact fans in marine and terrestrial environments.
1021 *Sedimentology*, 33, 677-698.

1022 Bowen, D.Q., Rose, J., McCabe, A.M., Sutherland, D.G. (1986). Correlation of quaternary glaciations
1023 in England, Ireland, Scotland and Wales. *Quaternary Science Reviews*, 5, 299-340.

1024 Bowen, D.Q., Phillips, F.M., McCabe, A.M., Knutz, P.C., Sykes, G.A. (2002). New data for the Last
1025 Glacial Maximum in Great Britain and Ireland. *Quaternary Science Reviews*, 21, 89-101.

1026 Bradwell, T., Stoker, M.S., Golledge, N.R., Wilson, C.K., Merritt, J.W., Long, D., Everest, J.D.,
1027 Hestvik, O.B., Stevenson, A.G., Hubbard, A.l., Finlayson, A.G., Mathers, H.E. (2008). The
1028 northern sector of the last British Ice Sheet: maximum extent and demise. *Earth-Science*
1029 *Reviews*, 88(3), 207-226.

1030 Broecker, W.S., Kennett, J.P., Flower, B.P., Teller, J.T., Trumbore, S., Bonani, G., Wolfli, W. (1989).
1031 The routing of Laurentide ice-sheet meltwater during the Younger Dryas cold event. *Nature*,
1032 341, 318–321.

1033 Chang, T.S., Flemming, B.W., Tilch, E., Bartholomä, A., Wöstmann, R. (2006). Late Holocene
1034 stratigraphic evolution of a back-barrier tidal basin in the East Frisian Wadden Sea, southern
1035 North Sea: transgressive deposition and its preservation potential. *Facies*, 52(3), 329-340.

1036 Clark, P.U., McCabe, A.M., Mix, A.C., Weaver, A.J., (2004). Rapid sea level rise at 19,000 years ago
1037 and its global implications. *Science*, (304), 1141–1144.

1038 Clark, J., McCABE, A., Schnabel, C., Clark, P.U., Freeman, S., Maden, C., Xu, S. (2009a). ^{10}Be
1039 chronology of the last deglaciation of County Donegal, northwestern Ireland. Boreas, 38(1),
1040 111-118.

1041 Clark, J., McCabe, A.M., Schnabel, C., Clark, P.U., McCarron, S., Freeman, S.P.H.T., Maden, C., Xu,
1042 S. (2009b). Cosmogenic Be-10 chronology of the last deglaciation of western Ireland, and
1043 implications for sensitivity of the Irish Ice Sheet to climate change. *Geological Society of*
1044 *America Bulletin*, 121 (1-2), 3-16.

1045 Clark, C.D., Hughes, A.L.C., Greenwood, S.L., Jordan, C., Sejrup, H.P. (2012a). Pattern and timing
1046 of retreat of the last British-Irish Ice Sheet. *Quaternary Science Reviews*, 44, 112-146.

1047 Clark, J., McCabe, A.M., Bowen, D.Q., Clark, P.U. (2012b). Response of the Irish Ice Sheet to abrupt
1048 climate change during the last deglaciation. *Quaternary Science Reviews*, 35, 100-115.

1049 Clarke, G.K. (2005). Subglacial processes. *Annu. Rev. Earth Planet. Sci., 33*, 247-276.

1050 Cook, A., Fox, A., Vaughan, D., Ferrigno, J. (2005). Retreating glacier fronts on the Antarctic
1051 Peninsula over the past half-century. *Science*, 308(5721), 541-544.

1052 Cowan, E.A., Cai, J., Powell, R.D., Clark, J.D., Pitcher, J.N. (1997). Temperate glacimarine varves:
1053 an example from Disenchantment Bay, southern Alaska. *Journal of Sedimentary Research*,
1054 67(3).

1055 Dansgaard, W., Johnsen, S.J., Clausen, H.B., Dahl-Jensen, D., Gundestrup, N.S., Hammer, C.U.,
1056 Hvidberg, C.S., Steffensen, J.P., Svelnbjörnsdottir, A.E., Jouzel, J., Bond, G. (1993).
1057 Evidence for general instability of past climate from a 250-kyr ice-core record. *Nature*,
1058 364(6434), 218-220.

1059 Dowdeswell, J.A., Villinger, H., Whittington, R.J., Marienfeld, P. (1993). Iceberg scouring in
1060 Scoresby Sund and on the East Greenland continental shelf. *Marine Geology*. 111, 37–53.

1061 Dowdeswell, J.A., Whittington, R.J., Marienfeld, P. (1994). The origin of massive diamicton facies by
1062 iceberg rafting and scouring, Scoresby Sund, East Greenland. *Sedimentology*, 41(1), 21-35.

1063 Dowdeswell, J., Maslin, M., Andrews, J., McCave, I. (1995). Iceberg production, debris rafting, and
1064 the extent and thickness of Heinrich layers (H-1, H-2) in North Atlantic sediments. *Geology*,
1065 23(4), 301-304.

1066 Dowdeswell, J., Whittington, R., Jennings, A., Andrews, J., Mackensen, A., Marienfeld, P. (2000). An
1067 origin for laminated glacimarine sediments through sea-ice build-up and suppressed iceberg
1068 rafting. *Sedimentology*, 47, 557-576.

1069 Dowdeswell, J., Ó Cofaigh, C., Pudsey, C. (2004). Continental slope morphology and sedimentary
1070 processes at the mouth of an Antarctic palaeo-ice stream. *Marine Geology*, 204(1), 203-214.

1071 Dowdeswell, J., Ottesen, D., Evans, J., Ó Cofaigh, C., Anderson, J. (2008). Submarine glacial
1072 landforms and rates of ice-stream collapse. *Geology*, 36(10), 819-822.

1073 Dunlop, P., Shannon, R., McCabe, M., Quinn, R., Doyle, E. (2010). Marine geophysical evidence for
1074 ice sheet extension and recession on the Malin Shelf: New evidence for the western limits of
1075 the British Irish Ice Sheet. *Marine Geology*, 276(1), 86-99.

1076 Evans, D.J.A., O'Cofaigh, C. (2003). Depositional evidence for marginal oscillations of the Irish Sea
1077 ice stream in southeast Ireland during the last glaciation. *Boreas*, 32(1), 76-101.

1078 Evans, J., Pudsey, C.J., O´Cofaigh, C., Morris, P., Domack, E. (2005). Late Quaternary glacial
1079 history, flow dynamics and sedimentation along the eastern margin of the Antarctic Peninsula
1080 ice sheet. *Quaternary science reviews*, 24, 741– 774.

1081 Evans, D.J.A., Phillips, E.R., Hiemstra, J.F., Auton, C.A. (2006). Subglacial till: formation,
1082 sedimentary characteristics and classification. *Earth-Science Reviews*, 78(1), 115-176.

1083 Evans, J., Dowdeswell, J.A., Ó Cofaigh, C., Benham, T.J., Anderson, J.B. (2006). Extent and
1084 dynamics of the West Antarctic Ice Sheet on the outer continental shelf of Pine Island Bay
1085 during the last glaciation. *Marine Geology*, 230(1), pp.53-72.

1086 Eyles, C.H. (1988). A model for striated boulder pavement formation on glaciated, shallow-marine
1087 shelves: an example from the Yakataga Formation, Alaska. *Journal of Sedimentary Research*,
1088 58(1), 62-71.

1089 Eyles, N., McCabe, A.M. (1989). The Late Devensian (< 22,000 BP) Irish Sea Basin: the sedimentary
1090 record of a collapsed ice sheet margin. *Quaternary Science Reviews*, 8(4), 307-351.

1091 Eyles, N., Eyles, C.H., Miall, A.D. (1983). Lithofacies types and vertical profile models; an
1092 alternative approach to the description and environmental interpretation of glacial diamict and
1093 diamictite sequences. *Sedimentology*, 30(3), 393-410.

1094 Feyling-Hanssen, R.W. (1972). The foraminifer Elphidium excavatum (Terquem) and its variant
1095 forms. *Micropaleontology*, 18(3), 337-354.

1096 Fischer, U., Clarke, G.K.C., Blatter, H., (1999). Evidence for temporally varying "sticky spots" at the
1097 base of Trapridge Glacier, Yukon Territory, Canada. *Journal of Glaciology*, 45, 352–360.

1098 Flemming, B., Schubert, H., Hertweck, G., Müller, K. (1992). Bioclastic tidal-channel lag deposits: a
1099 genetic model. *Senckenbergiana marit*, 22, 109-129.

1100 Fyfe, J.A., Long, D. Evans, D. (1993) The geology of the Malin-Hebrides Sea area. *British*
1101 *Geological Survey, United Kingdom, Offshore Regional Report*. HMSO, London.

1102 Glasser, N.F., Scambos, T.A., Bohlander, J., Truffer, M., Pettit, E., Davies, B.J. (2011). From ice-
1103 shelf tributary to tidewater glacier: continued rapid recession, acceleration and thinning of
1104 Röhss Glacier following the 1995 collapse of the Prince Gustav Ice Shelf, Antarctic
1105 Peninsula. *Journal of Glaciology*, 57(203), 397-406.

1106 Greenwood, S.L., Clark, C.D. (2008). Subglacial bedforms of the Irish ice sheet. *Journal of Maps*,
1107 4(1), 332-357.

1108 Greenwood, S.L., Clark, C.D. (2009). Reconstructing the last Irish Ice Sheet 2: a geomorphologically-
1109 driven model of ice sheet growth, retreat and dynamics. *Quaternary Science Reviews*, 28(27-
1110 28), 3101-3123.

1111 Grobe, H. (1987). A simple method for the determination of ice-rafted debris in sediment cores.
1112 *Polarforschung*, 57(3), 123-126.

1113 Hald, M., Korsun, S. (1997). Distribution of modern benthic foraminifera from fjords of Svalbard,
1114 European Arctic. *Journal of Foraminiferal Research*. 27(2), 101–122.

1115 Hald, M., Steinsund, P.I., Dokken, T., Korsun, S., Polyak, L., Aspeli, R., (1994). Recent and late
1116 Quarternary distribution of Elphidium excavatum f. clavata in Arctic seas. *Cushman*
1117 *Foundation Special Publication*, 32, 141–153.

1118 Hill, J.C., Gayes, P.T., Driscoll, N.W., Johnstone, E.A., Sedberry, G.R. (2008). Iceberg scours along
1119 the southern US Atlantic margin. *Geology*, 36(6), 447-450.

1120 Hillenbrand, C.D., Baesler, A., Grobe, H. (2005). The sedimentary record of the last glaciation in the
1121 western Bellingshausen Sea (West Antarctica): implications for the interpretation of
1122 diamictons in a polar-marine setting. *Marine geology*, 216(4), 191-204.

1123 Hillenbrand, C.D., Larter, R.D., Dowdeswell, J.A., Ehrmann, W., Ó Cofaigh, C., Benetti, S., Grobe,
1124 H. (2010). The sedimentary legacy of a palaeo-ice stream on the shelf of the southern
1125 Bellingshausen Sea: Clues to West Antarctic glacial history during the Late Quaternary.
1126 *Quaternary Science Reviews*, 29(19), 2741-2763.

1127 Hillenbrand, C.-D., Kuhn, G., Smith, J.A., Gohl, K., Graham, A.G., Larter, R.D., Klages, J.P.,
1128 Downey, R., Moreton, S.G., Forwick, M., Vaughan, D.G. (2013). Grounding-line retreat of
1129 the west Antarctic ice sheet from inner Pine island Bay. *Geology*, 41(1), 35-38.

Howat, I.M., Domack, E.W. (2003). Reconstructions of western Ross Sea palaeo-ice-stream grounding zones from high-resolution acoustic stratigraphy. *Boreas*, 32(1), 56-75.

Jakobsson, M., Anderson, J.B., Nitsche, F.O., Dowdeswell, J.A., Gyllencreutz, R., Kirchner, N., Mohammad, R., O'Regan, M., Alley, R.B., Anandakrishnan, S., Eriksson, B., Kirshner, A., Fernandez, R., Stolldorf, T., Minzoni, R., Majewski, W. (2011). Geological record of ice shelf break-up and grounding line retreat, Pine Island Bay, West Antarctica. *Geology*, 39(7), 691-694.

Jónsson, S.A., Schomacker, A., Benediktsson, Í.Ö., Ingólfsson, Ó., Johnson, M.D. (2014). The drumlin field and the geomorphology of the Múlajökull surge-type glacier, central Iceland. *Geomorphology*, 207, 213-220.

Kamb, B. (2001). Basal zone of the West Antarctic ice streams and its role in lubrication of their rapid motion. *The West Antarctic ice sheet: behavior and environment*, 157-199.

Kilfeather, A.A., Ó Cofaigh, C., Lloyd, J.M., Dowdeswell, J.A., Xu, S., Moreton, S.G. (2011). Ice-stream retreat and ice-shelf history in Marguerite Trough, Antarctic Peninsula: Sedimentological and foraminiferal signatures. *Geological Society of America Bulletin*, 123(5-6), 997-1015.

Larter, R.D., Gohl, K., Hillenbrand, C.D., Kuhn, G., Deen, T., Dietrich, R., Eagles, G., Johnson, J., Livermore, R., Nitsche, F., Pudsey, C., Schenke, H.W., Smith, J., Udintsev, G., Uenzelmann-Neben, G. (2007). West Antarctic Ice Sheet change since the last glacial period. *Eos, Transactions American Geophysical Union*, 88(17), 189-190.

Lecavalier, B.S., Milne, G.A., Simpson, M.J., Wake, L., Huybrechts, P., Tarasov, L., Kjeldsen, K.K., Funder, S., Long, A.J., Woodroffe, S., Dyke, A.S. (2014). A model of Greenland ice sheet deglaciation constrained by observations of relative sea level and ice extent. *Quaternary science reviews*, 102, 54-84.

1154 Lian, O.B., Hicock, S.R. (2000). Thermal conditions beneath parts of the last Cordilleran Ice Sheet
1155 near its centre as inferred from subglacial till, associated sediments, and bedrock. *Quaternary*
1156 *International*, *68*, 147-162.

1157 Löwemark, L., Chao, W.S., Gyllencreutz, R., Hanebuth, T.J., Chiu, P.Y., Yang, T.N., Su, C.C.,
1158 Chuang, C.K., Dominguez, D.C.L., Jakobsson, M. (2015). Variations in glacial and
1159 interglacial marine conditions over the last two glacial cycles off northern Greenland.
1160 *Quaternary Science Reviews*. ISSN: 0277-3791.

1161 Lucchi, R., Camerlenghi, A., Rebesco, M., Colmenero-Hidalgo, E., Sierro, F., Sagnotti, L., Urgeles,
1162 R., Melis, R., Morigi, C., Bárcena, M.-A., Giorgetti, G., Villa, G., Persico, D., Flores, J.-A.,
1163 Rigual-Hernández, A.S., Pedrosa, M.T., Macri, P., Caburlotto, A. (2013). Postglacial
1164 sedimentary processes on the Storfjorden and Kveithola trough mouth fans: Significance of
1165 extreme glacimarine sedimentation. *Global and Planetary Change*, 111, 309-326.

1166 McCabe, A.M. (1986). Glaciomarine facies deposited by retreating tidewater glaciers: an example
1167 from the Late Pleistocene of Northern Ireland. *Journal of Sedimentary Research*, 56(6).

1168 McCabe, A.M., Clark, P.U. (1998). Ice-sheet variability around the North Atlantic Ocean during the
1169 last deglaciation. *Nature*, 392(6674), 373-377.

1170 McCabe, A., Clark, P.U. (2003). Deglacial chronology from County Donegal, Ireland: implications
1171 for deglaciation of the British–Irish ice sheet. *Journal of the Geological Society*, 160(6), 847-
1172 855.

1173 McCabe, A., Clark, P., Clark, J. (2005). AMS C-14 dating of deglacial events in the Irish Sea Basin
1174 and other sectors of the British–Irish ice sheet. *Quaternary Science Reviews*, 24(14), 1673-
1175 1690.

1176 McCabe, A.M., Clark, P.U., Clark, J. (2007). Radiocarbon constraints on the history of the western
1177 Irish ice sheet prior to the Last Glacial Maximum. *Geology*, 35(2), 147-150.

Melis, R., Salvi, G. (2009). Late Quaternary foraminiferal assemblages from western Ross Sea (Antarctica) in relation to the main glacial and marine Lithofacies. *Marine Micropaleontology*, 70(1–2), 39-53.

Mudie, P.J., Keen, C.E., Hardy, I.A., Vis, G. (1984). Multivariate analysis and quantitative paleoecology of benthic foraminifera in surface and Late Quaternary shelf sediments, northern Canada. *Micropaleontology*, 8, 283-313.

Ó Cofaigh, C., Dowdeswell, J.A. (2001). Laminated sediments in glacimarine environments: diagnostic criteria for their interpretation. *Quaternary Science Reviews*, 20(13), 1411-1436.

Ó Cofaigh, C., Evans, D.J. (2001). Deforming bed conditions associated with a major ice stream of the last British ice sheet. *Geology*, 29(9), 795-798.

Ó Cofaigh, C., Evans, D.J. (2007). Radiocarbon constraints on the age of the maximum advance of the British–Irish Ice Sheet in the Celtic Sea. *Quaternary Science Reviews*, 26(9), 1197-1203.

Ó Cofaigh, C., Taylor, J., Dowdeswell, J.A., Rosell-Mele´, A., Kenyon, N.H., Evans, J., Mienert, J. (2002). Geological evidence for sediment reworking on high-latitude continental margins and its implications for palaeoceanography: insights from the Norwegian-Greenland Sea. In: Dowdeswell, J.A.,O´Cofaigh, C. (Eds.), Glacier-influenced Sedimentation on High-latitude Continental Margins. *Geological Society of London, Special Publication*, 203, 325–348.

Ó Cofaigh, C., Dowdeswell, J.A., Allen, C.S., Hiemstra, J.F., Pudsey, C.J., Evans, J., Evans, D.J.A. (2005). Flow dynamics and till genesis associated with a marine-based Antarctic palaeo-ice stream. *Quaternary Science Reviews*, 24, 709– 740.

Ó Cofaigh, C., Evans, J., Dowdeswell, J.A., Larter, R.D. (2007). Till characteristics, genesis and transport beneath Antarctic paleo-ice streams. *Journal of Geophysical Research*: *Earth Surface*, 112(F3).

1201 Ó Cofaigh, C., Dunlop, P., Benetti, S. (2010). Marine geophysical evidence for Late Pleistocene ice
1202 sheet extent and recession off northwest Ireland. *Quaternary Science Reviews*, 44, 147-159.

1203 Ó Cofaigh, C., Evans, D.J.A., Hiemstra, J.F. (2011). Formation of a stratified subglacial 'till'
1204 assemblage by ice-marginal thrusting and glacier overriding. *Boreas*, 40(1), 1-14.

1205 Ó Cofaigh, C., Telfer, M.W., Bailey, R.M., Evans, D.J. (2012). Late Pleistocene chronostratigraphy
1206 and ice sheet limits, southern Ireland. *Quaternary Science Reviews*, 44, 160-179.

1207 Ottesen, D., Rise, L., Knies, J., Olsen, L., Henriksen, S. (2005). The Vestfjorden-Trænadjupet palaeo-
1208 ice stream drainage system, mid-Norwegian continental shelf. *Marine Geology*, 218(1), 175-
1209 189.

1210 Peck, V., Hall, I., Zahn, R., Elderfield, H., Grousset, F., Hemming, S., Scourse, J. (2006). High
1211 resolution evidence for linkages between NW European ice sheet instability and Atlantic
1212 Meridional Overturning Circulation. *Earth and Planetary Science Letters*, 243(3), 476-488.

1213 Peters, J.L., Benetti, S., Dunlop, P., Ó Cofaigh, C. (2015). Maximum extent and dynamic behaviour
1214 of the last British–Irish Ice Sheet west of Ireland. *Quaternary Science Reviews*, 128, 48-68.

1215 Polyak, L., Gataullin, V., Gainanov, V., Gladysh, V., Goremykin, Yu. (2002). Kara Sea expedition
1216 yields insight into LGM ice sheet extent. *Eos 83*, 46, 525–529.

1217 Praeg, D., McCarron, S., Dove, D., Ó Cofaigh, C., Scott, G., Monteys, X., Facchin, L., Romeo, R.,
1218 Coxon, P. (2015). Ice sheet extension to the Celtic Sea shelf edge at the Last Glacial
1219 Maximum. *Quaternary Science Reviews*, 111, 107-112.

1220 Reimer, P.J., Bard, E., Bayliss, A., Beck, J.W., Blackwell, P.G., Ramsey, C.B., Buck, C.E., Hai, C.,
1221 Edwards, R.L., Friedrich, M., Grootes, P.M., Guilderson, T.P., Haflidason, H., Hajdas, I.,
1222 Hatté, C., Heaton, T.J., Hoffmann, D.L., Hogg, A.G., Hughen, K.A., Kaiser, K.F., Kromer,
1223 B., Manning, S.W., Niu, M., Reimer, R.W., Richards, D.A., Scott, E.M., Southon, J.R., Staff,

R.A., Turney, C.S.M., van der Plicht, J. (2013). IntCal13 and Marine13 radiocarbon age calibration curves 0-50,000 years cal BP. *Radiocarbon*, 55(4), 1869–1887.

Rignot, E., Koppes, M., Velicogna, I. (2010). Rapid submarine melting of the calving faces of West Greenland glaciers. *Nature Geoscience*, 3(3), 187-191.

Rignot, E., Velicogna, I., Van den Broeke, M.R., Monaghan, A., Lenaerts, J.T.M. (2011). Acceleration of the contribution of the Greenland and Antarctic ice sheets to sea level rise. *Geophysical Research Letters*, 38(5).

Rijsdijk, K.F., Owen, G., Warren, W.P., McCarroll, D., van der Meer, J.J. (1999). Clastic dykes in over-consolidated tills: evidence for subglacial hydrofracturing at Killiney Bay, eastern Ireland. *Sedimentary Geology*, 129(1), 111-126.

Robinson, S.G., Maslin, M.A., McCave, I.N. (1995). Magnetic susceptibility variations in late Pleistocene deep-sea sediments of the N.E. Atlantic: implications for ice-rafting and paleocirculation at the last Glacial Maximum. *Paleoceanography*, 10, 221-250.

Robinson, A., Calov, R., Ganopolski, A. (2011). Greenland ice sheet model parameters constrained using simulations of the Eemian Interglacial. *Climate of the Past*, 7(2), 381-396.

Saito, Y., Katayama, H., Ikehara, K., Kato, Y., Matsumoto, E., Oguri, K., Oda, M., Yumoto, M. (1998). Transgressive and highstand systems tracts and post-glacial transgression, the East China Sea. *Sedimentary Geology*, 122(1), 217-232.

Scambos, T.A., Bohlander, J.A., Shuman, C.U., Skvarca, P. (2004). Glacier acceleration and thinning after ice shelf collapse in the Larsen B embayment, Antarctica. *Geophysical Research Letters*, 31(18), 1-4.

Scourse, J.D., Austin, W.E.N., Bateman, R.M., Catt, J.A., Evans, C.D.R., Robinson, J.E., Young, J.R. (1990). Sedimentology and micropalaeontology of glacimarine sediments from the central

and southwestern Celtic Sea. *Geological Society, London, Special Publications*, 53(1), 329-347.

Scourse, J.D., Haapaniemi, A.I., Colmenero-Hidalgo, E., Peck, V.L., Hall, I.R., Austin, W.E., Knutz, P.C., Zahn, R. (2009). Growth, dynamics and deglaciation of the last British–Irish ice sheet: the deep-sea ice-rafted detritus record. *Quaternary Science Reviews*, 28(27), 3066-3084.

Sejrup, H.P., Haflidason, H., Aarseth, I., King, E., Forsberg, C.F., Long, D., Rokoengen, K. (1994). Late Weichselian glaciation history of the northern North Sea. *Boreas*, 23(1), 1-13.

Sejrup, H.P., Hjelstuen, B.O., Dahlgren, K.I.T., Haflidason, H., Kuijpers, A., Nygård, A., Praeg, D., Stoker, M.S., Vorren, T.O. (2005). Pleistocene glacial history of the NW European continental margin. *Marine and Petroleum Geology*, 22, 1111–1129.

Sharp, M. (1982). Modification of clasts in lodgement tills by glacial erosion. *Journal of Glaciology*, 28(100), 475-481.

Shevenell, A.E., Domack, E.W., Kernan, G.M. (1996). Record of Holocene palaeoclimate change along the Antarctic Peninsula: evidence from glacial marine sediments, Lallemand Fjord. *Papers and Proceedings of the Royal Society of Tasmania*, 130(2), 55-64.

Ship, S., Anderson, J., & Domack, E. (1999). Late Pleistocene–Holocene retreat of the West Antarctic Ice-Sheet system in the Ross Sea: part 1—geophysical results. Geological Society of America Bulletin, 111(10), 1486-1516.

Shipp, S.S., Wellner, J.S., Anderson, J.B. (2002). Retreat signature of a polar ice stream: sub-glacial geomorphic features and sediments from the Ross Sea, Antarctica. Special Publication-Geological Society of London, 203, 277-304.

Smeulders, G.G.B., Koho, K.A., de Stigter, H.C., Mienis, F., de Haas, H., van Weering, T.C.E. (2014). Cold-water coral habitats of Rockall and Porcupine Bank, NE Atlantic Ocean:

Sedimentary facies and benthic foraminiferal assemblages. *Deep Sea Research Part II: Topical Studies in Oceanography*, 99, 270-285.

Smith, J.A., Hillenbrand, C.D., Kuhn, G., Larter, R.D., Graham, A.G., Ehrmann, W., Moreton, S.G., Forwick, M. (2011). Deglacial history of the West Antarctic Ice Sheet in the western Amundsen Sea embayment. *Quaternary Science Reviews*, 30(5), 488-505.

Stalder, C., Spezzaferri, S., Rüggeberg, A., Pirkenseer, C., Gennari, G. (2014). Late Weichselian deglaciation and early Holocene development of a cold-water coral reef along the Lopphavet shelf (Northern Norway) recorded by benthic foraminifera and ostracoda. *Deep Sea Research Part II: Topical Studies in Oceanography*, 99, 249-269.

Stuiver, M., Reimer, P.J. (1993). Extended ^{14}C database and revised CALIB radiocarbon calibration program. *Radiocarbon*, 35, 215-230.

Syvitski, J.P.M., Andrews, J.T., Dowdeswell, J.A. (1996). Sediment deposition in an iceberg-dominated glacimarine environment, East Greenland: basin fill implications. *Global and Planetary Change*, 12(1), pp.251-270.

Sættem, J., Rise, L., Rokoengen, K., By, T. (1996). Soil investigations, offshore mid Norway: A case study of glacial influence on geotechnical properties. *Global and Planetary Change*, 12(1), 271-285.

van der Meer, J.J., Kjaer, K.H., Krüger, J. (1999). Subglacial water-escape structures and till structures, sléttjökull, Iceland. *Journal of Quaternary Science*, 14(3), 191-205.

van der Meer, J.J., Menzies, J., Rose, J. (2003). Subglacial till: the deforming glacier bed. *Quaternary Science Reviews*, 22(15), 1659-1685.

van der Wateren, F.M. (1995). Structural geology and sedimentology of push moraines: processes of soft sediment deformation in a glacial environment and the distribution of glaciotectonic styles. *Meded. Rijks Geol. Dienst, Geological Survey of The Netherlands, Haarlem*, 54.

1295 Viana, A., Faugères, J.-C., Stow, D. (1998). Bottom-current-controlled sand deposits—a review of
1296 modern shallow-to deep-water environments. *Sedimentary Geology*, 115(1), 53-80.

1297 Vorren, T.O., Hald, M ., Edvardsemn,. Lind-Hansen, O.W. (1983). Glacigenic sediments and
1298 sedimentary environments on continental shelves: general principles with a case study from
1299 the Norwegian shelf. In: *Glacial Deposits in North- West Europe.* Ehlers, J. (Ed.), pp. 61-73.
1300 Balkema, Rotterdam.

1301 Wellner, J., Lowe, A., Shipp, S., Anderson, J. (2001). Distribution of glacial geomorphic features on
1302 the Antarctic continental shelf and correlation with substrate: implications for ice behavior.
1303 *Journal of Glaciology*, 47(158), 397-411.

1304 Wilson, L. J., Austin, W. E., & Jansen, E. (2002). The last British Ice Sheet: growth, maximum extent
1305 and deglaciation. *Polar Research*, 21(2), 243-250.

1306

Figure

Click here to download high resolution image

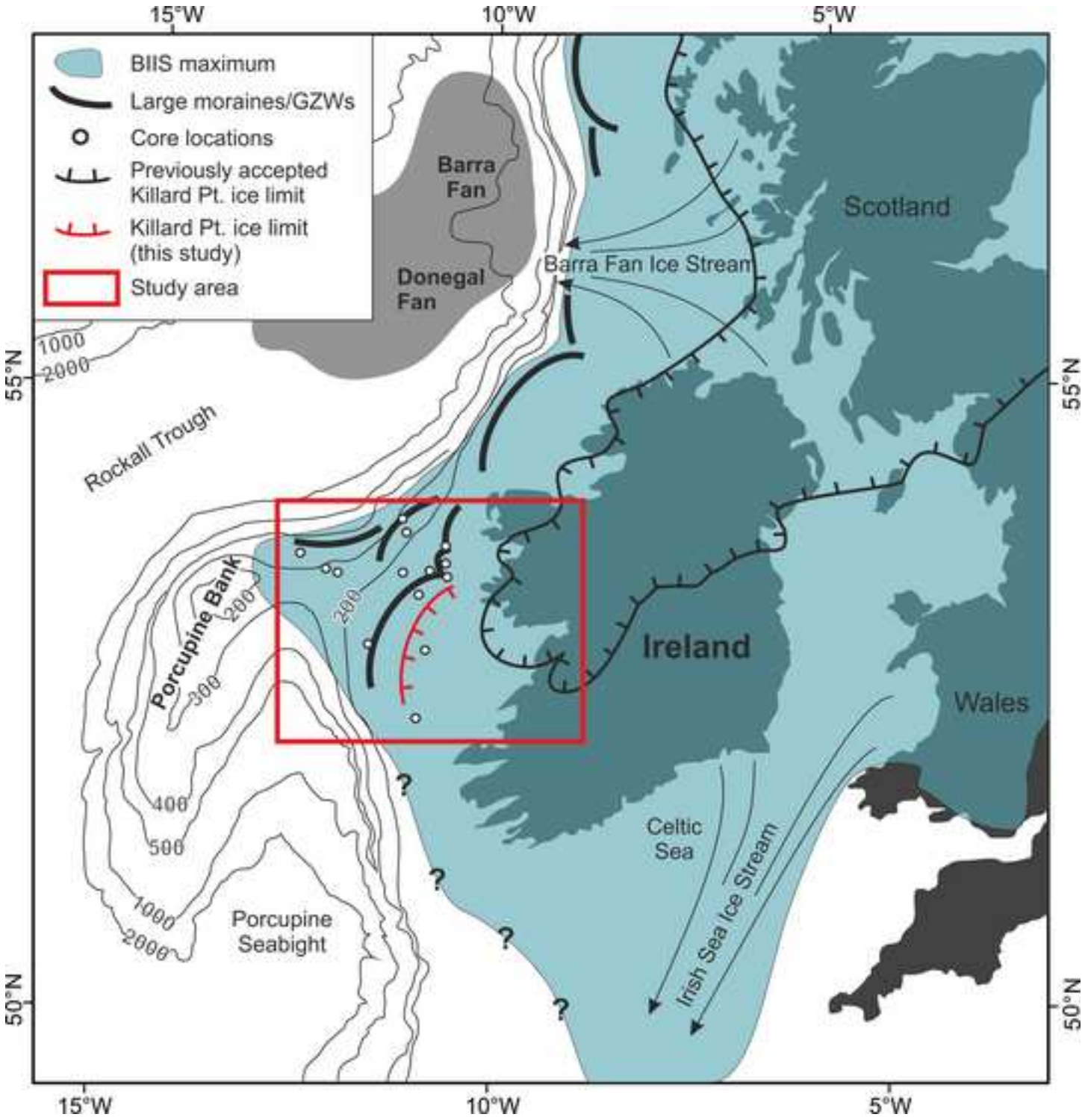

Figure

Click here to download high resolution image

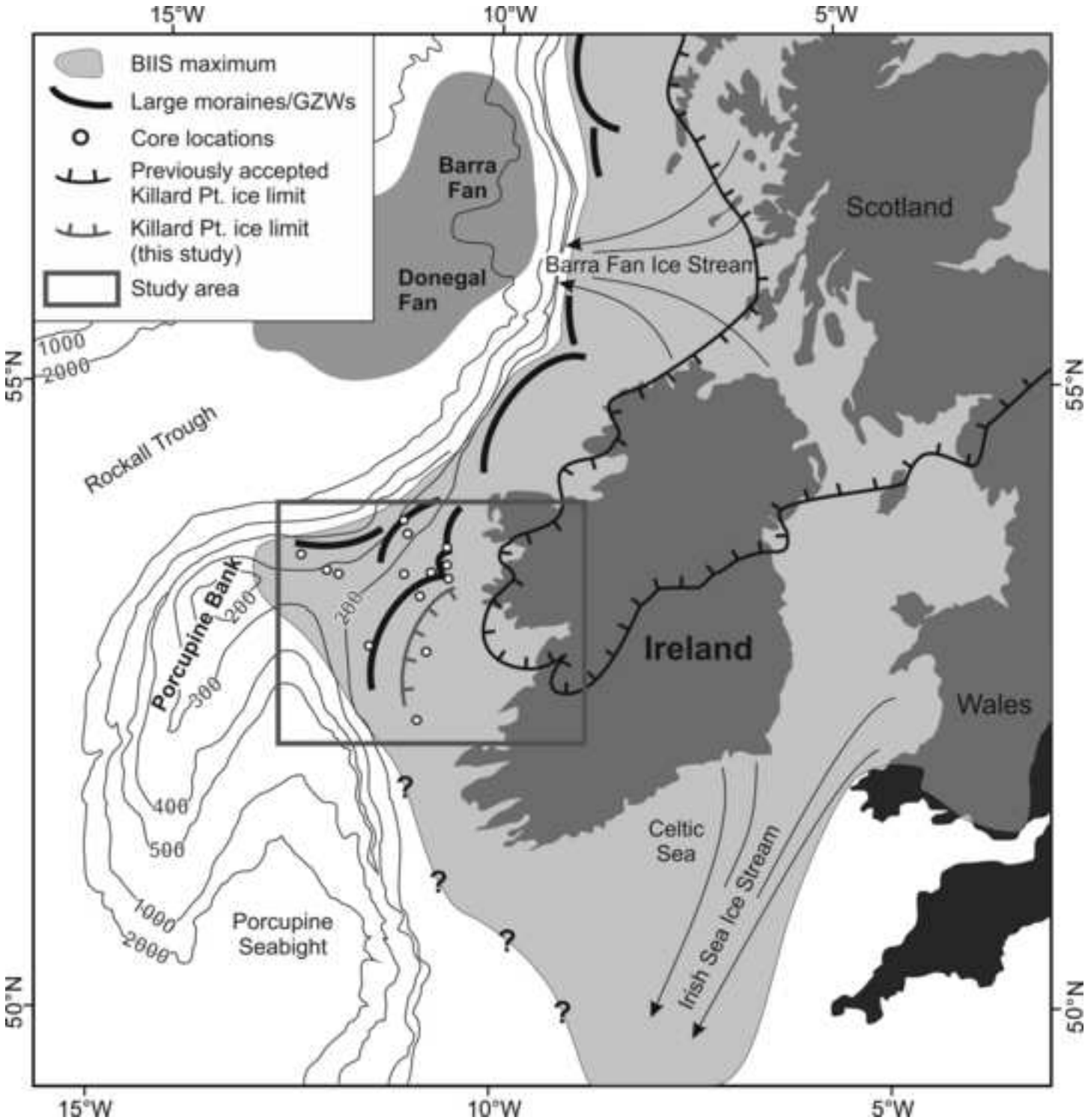

Figure

Click here to download high resolution image

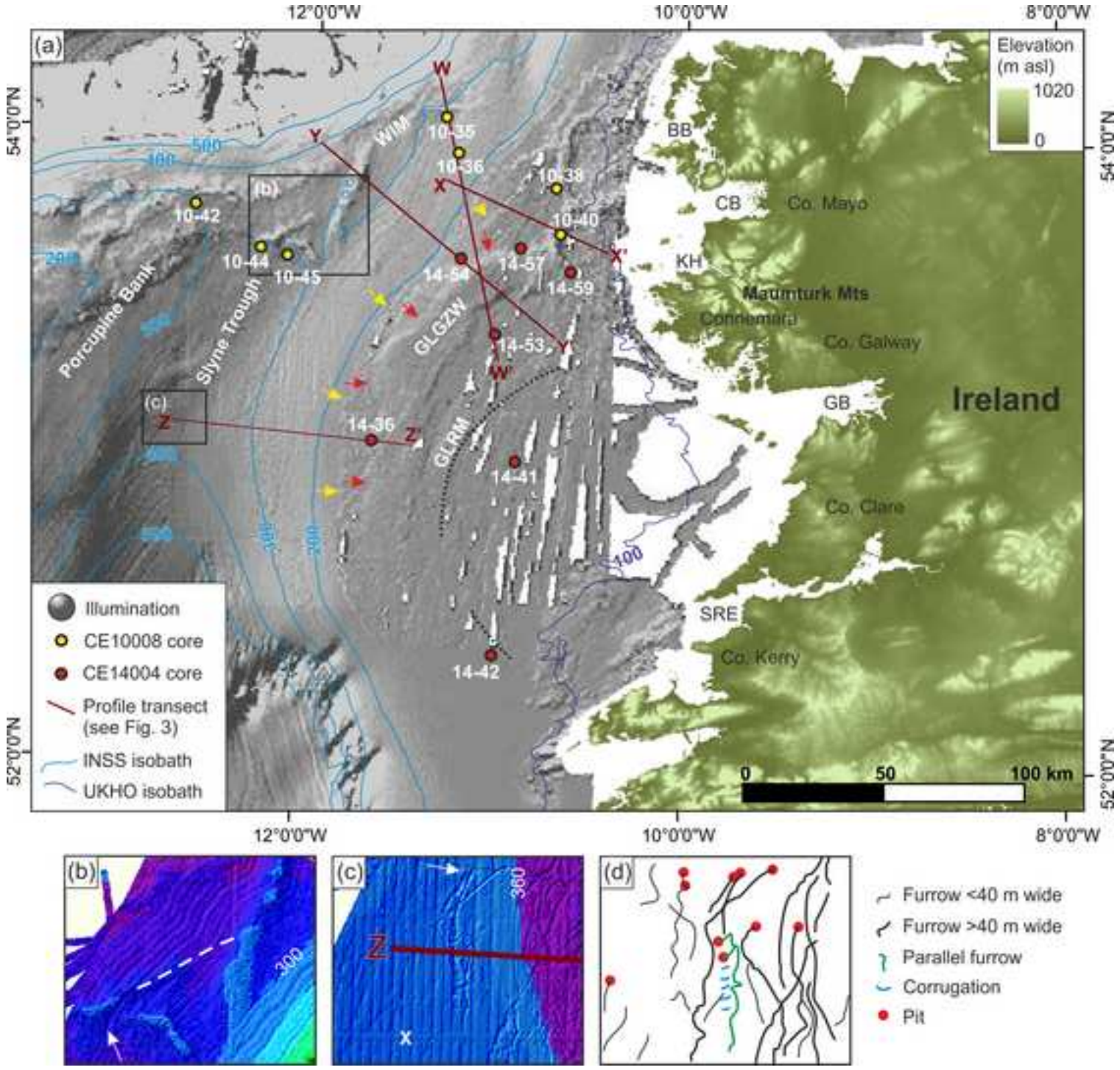

Figure

Click here to download high resolution image

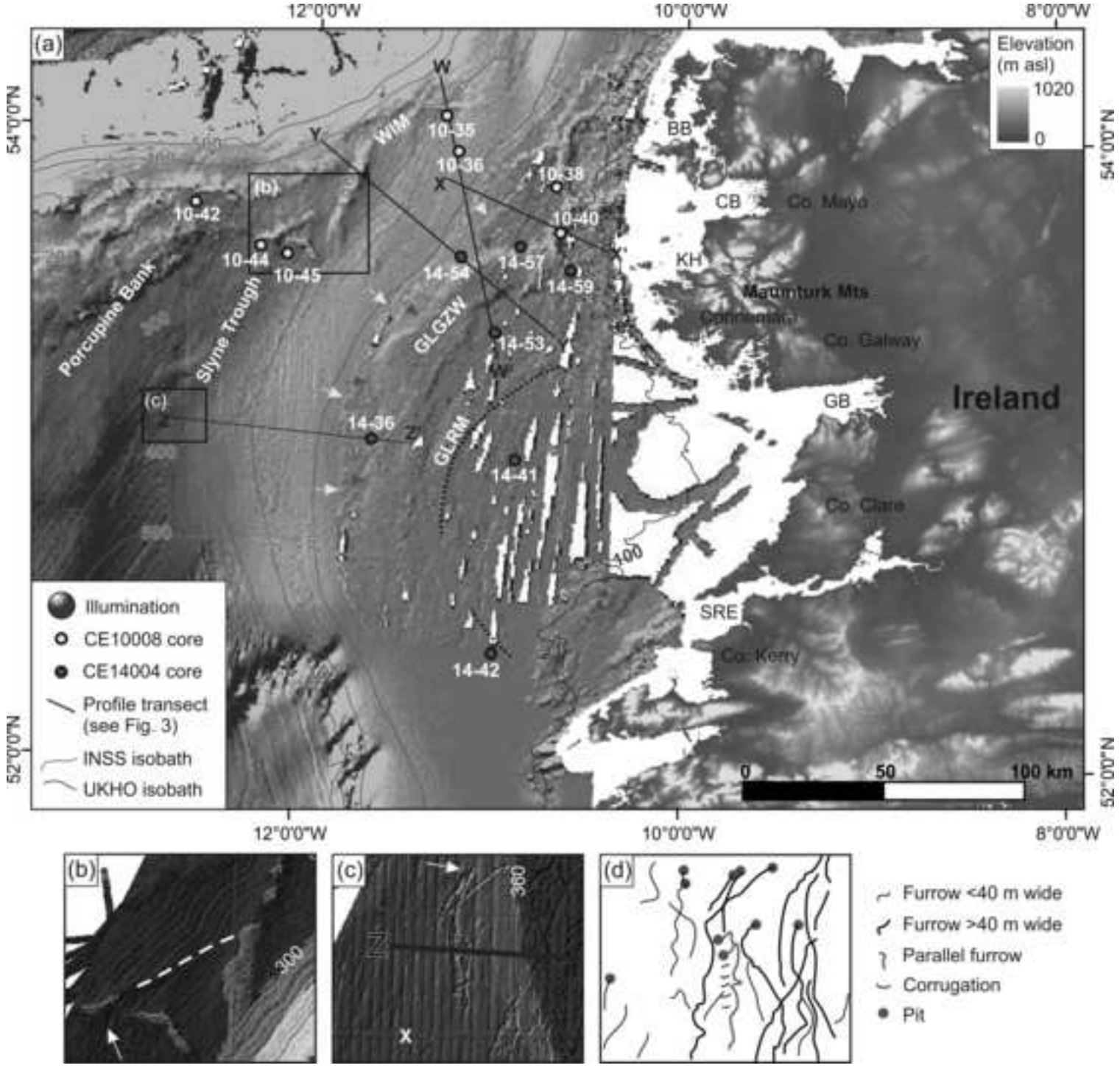

Figure

Click here to download high resolution image

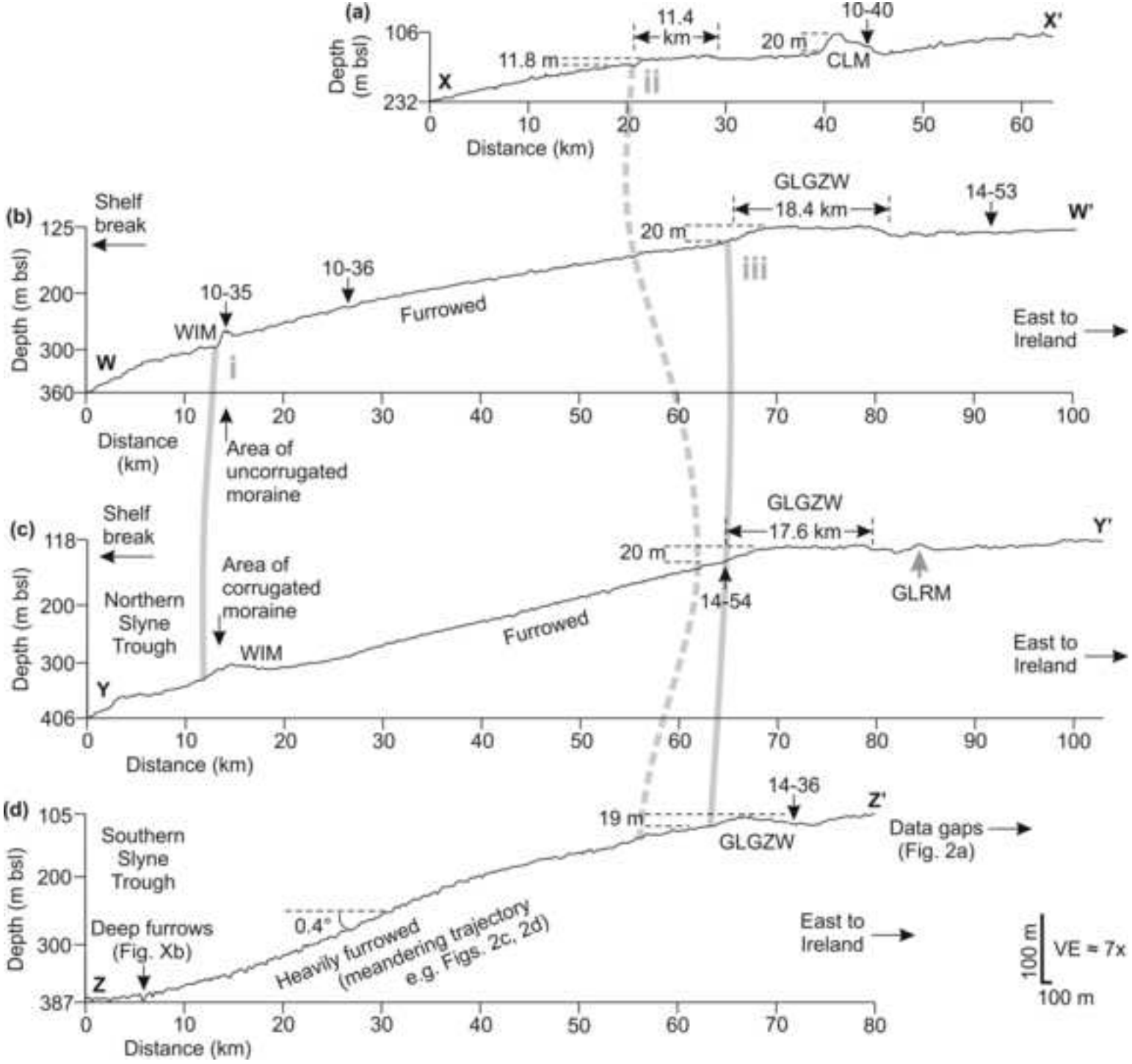

Figure

Click here to download high resolution image

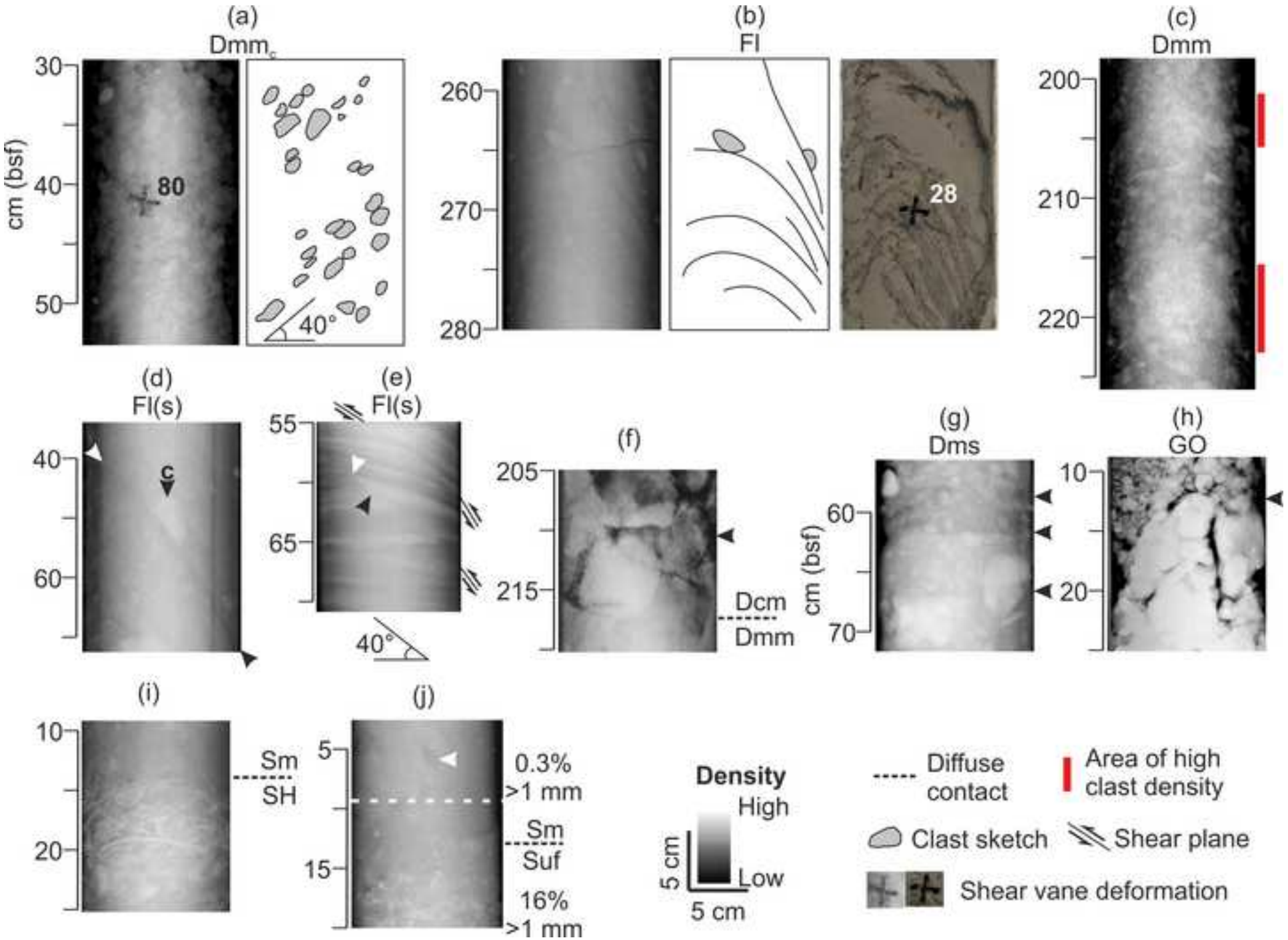

Figure

Click here to download high resolution image

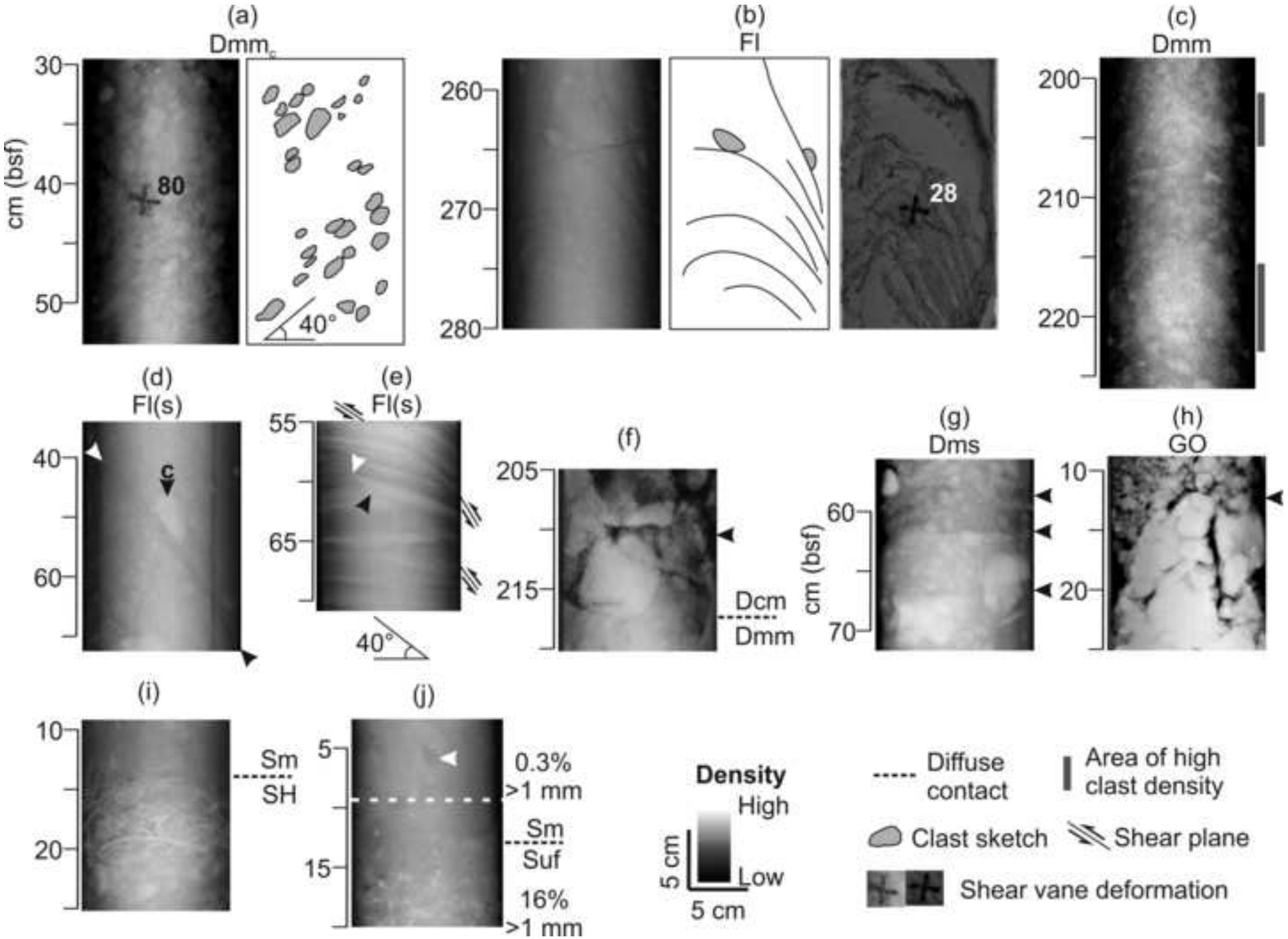

Figure

Click here to download high resolution image

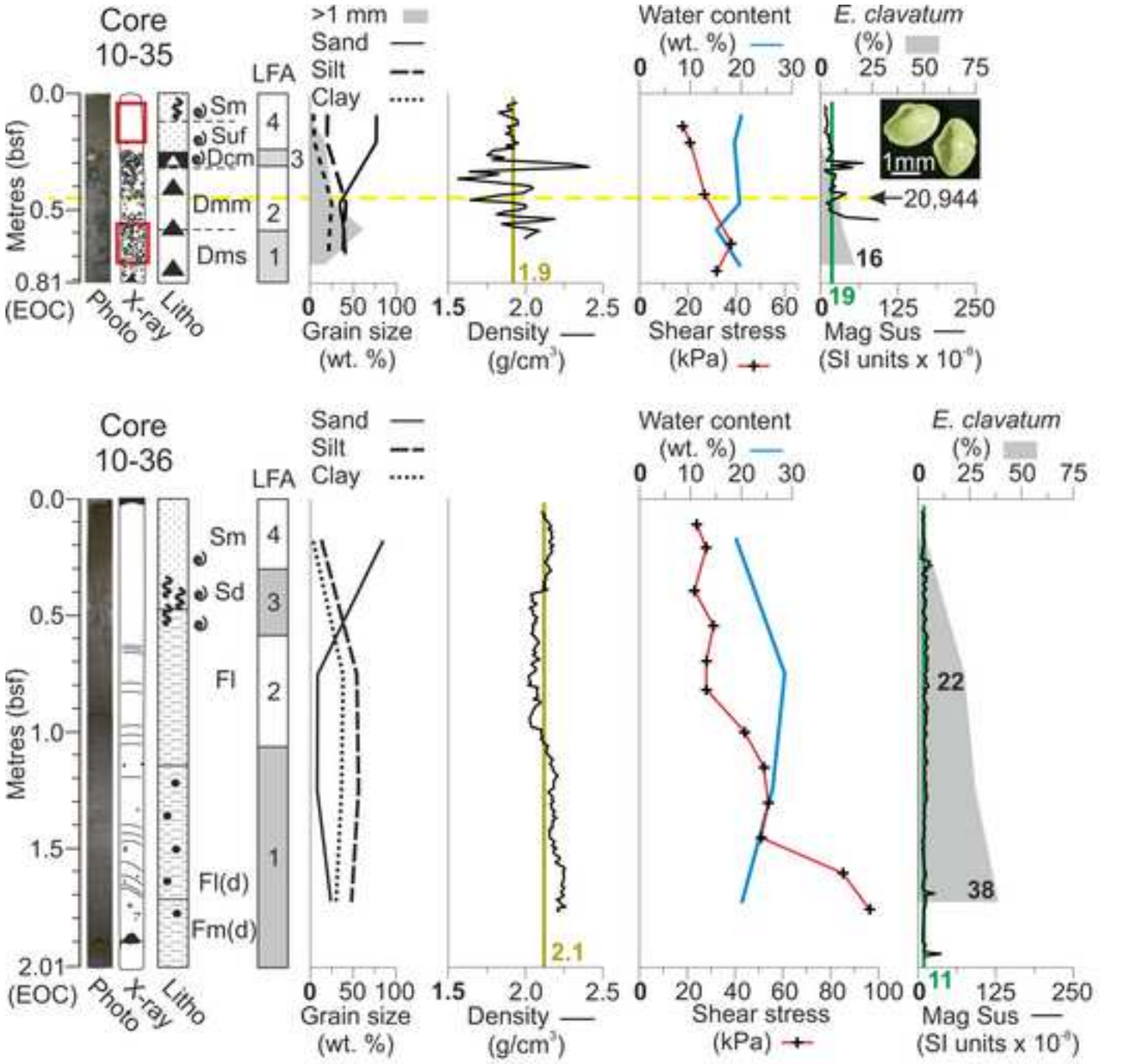

Legend

X-ray sketch

- Clast
- Laminae
- Shell/fragment
- Coring Deformation
- Fig. 4 ref.

Lithology / sedimentology

- Sand
- Gravel
- Mud
- Diamicton
- Dcm diamicton
- Shell hash
- Bioturbation
- Shell/frag.
- Dropstone
- Soft-sediment clast
- Sharp contact
- Gradational contact
- Clast with glacigenic wear features
- Unconformity
- Dewatering structures
- Shear plane

General

- S.S. measurement
- Excluded (in mean) Mag Sus measurements
- Mag Sus mean
- Density mean
- Cal. ^{14}C age

Figure

Click here to download high resolution image

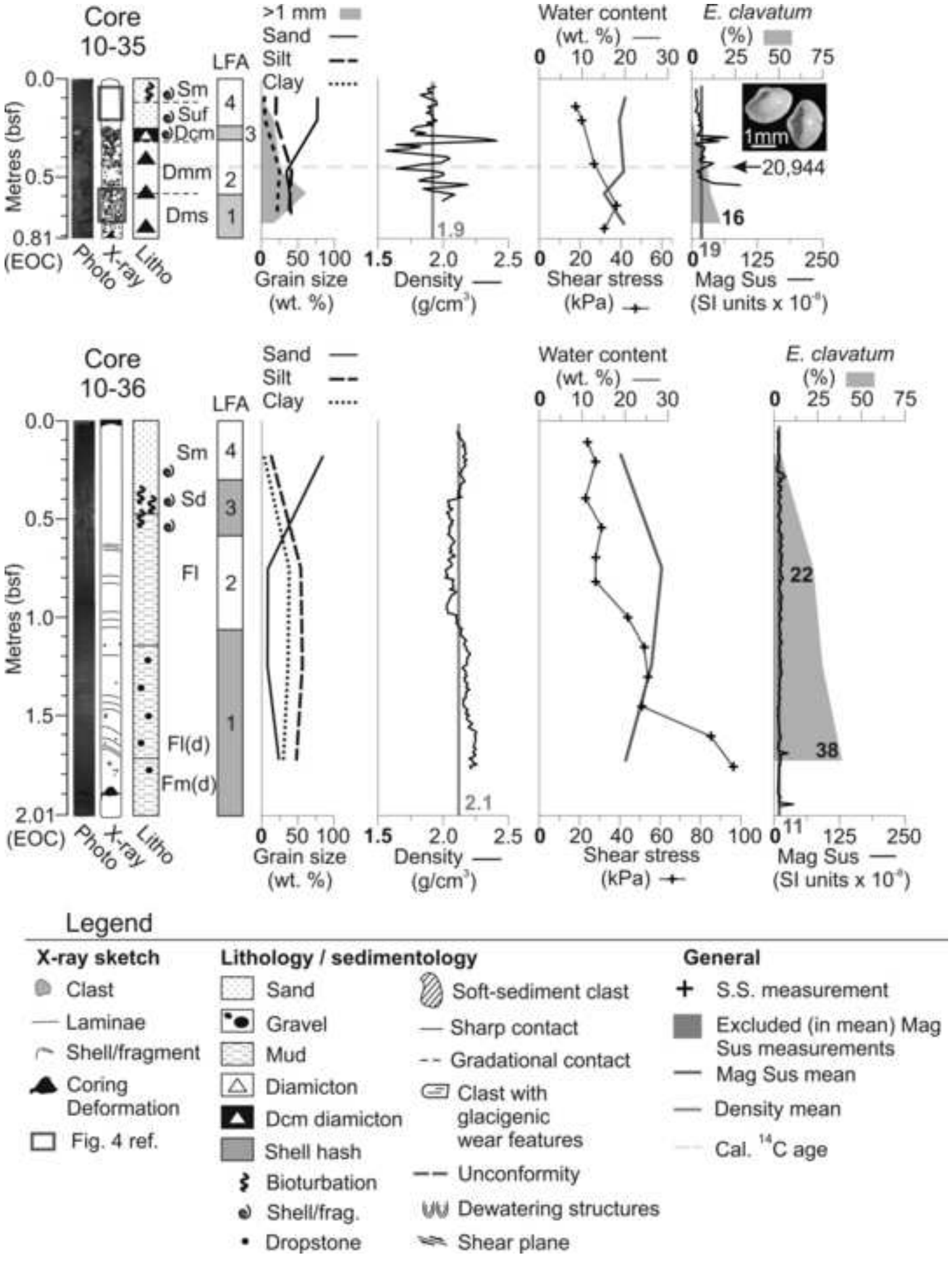

Figure

Click here to download high resolution image

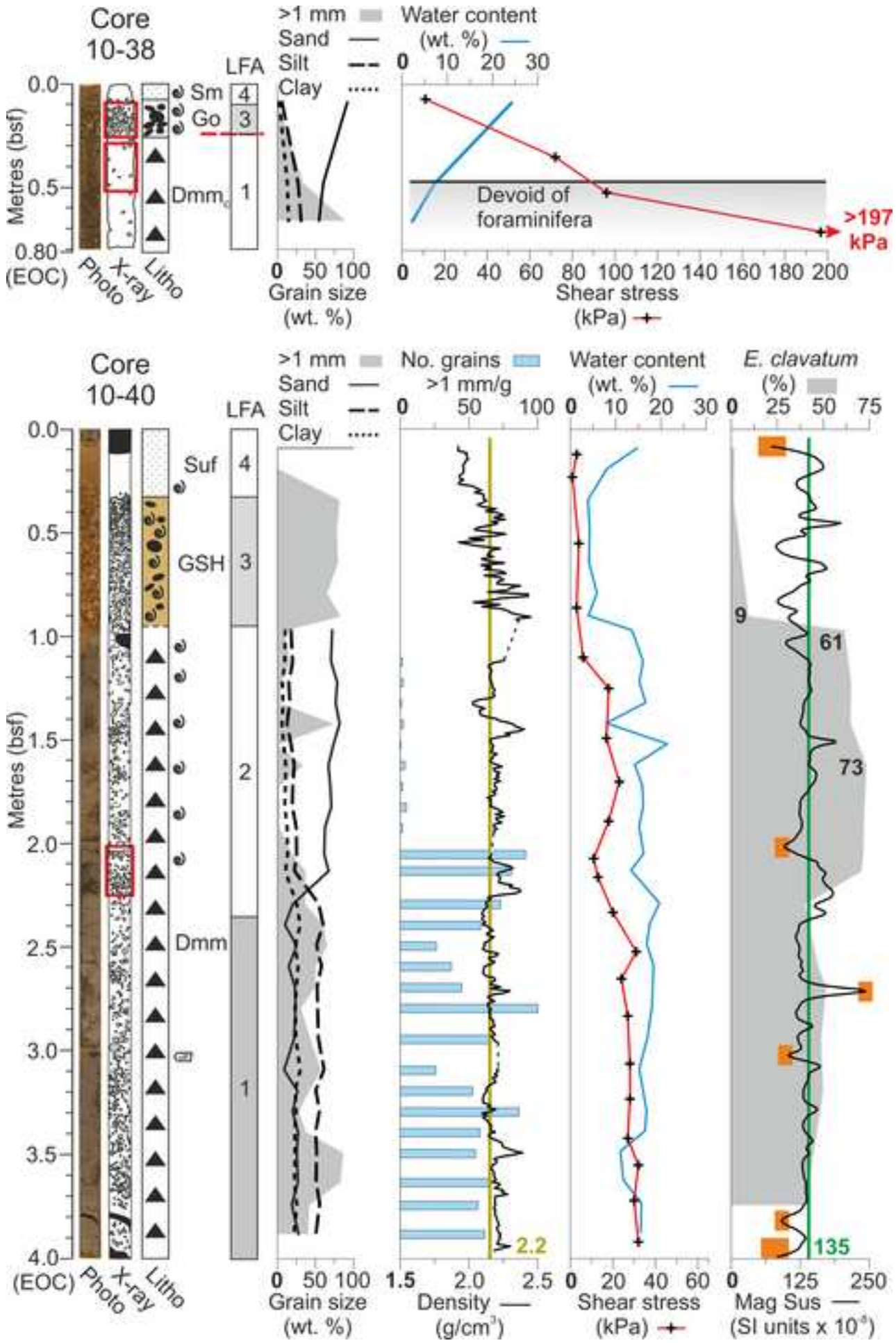

Figure

Click here to download high resolution image

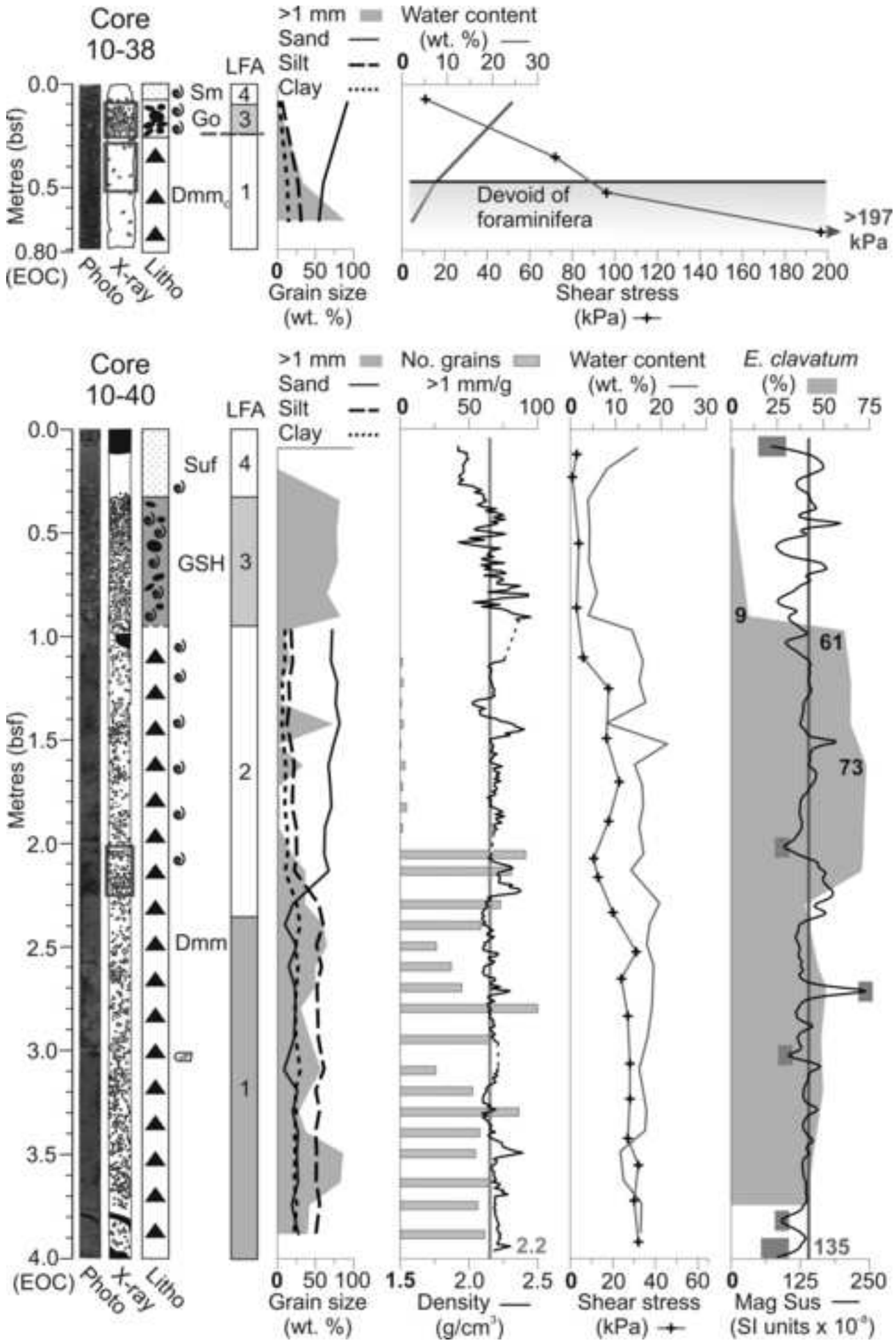

Figure

Click here to download high resolution image

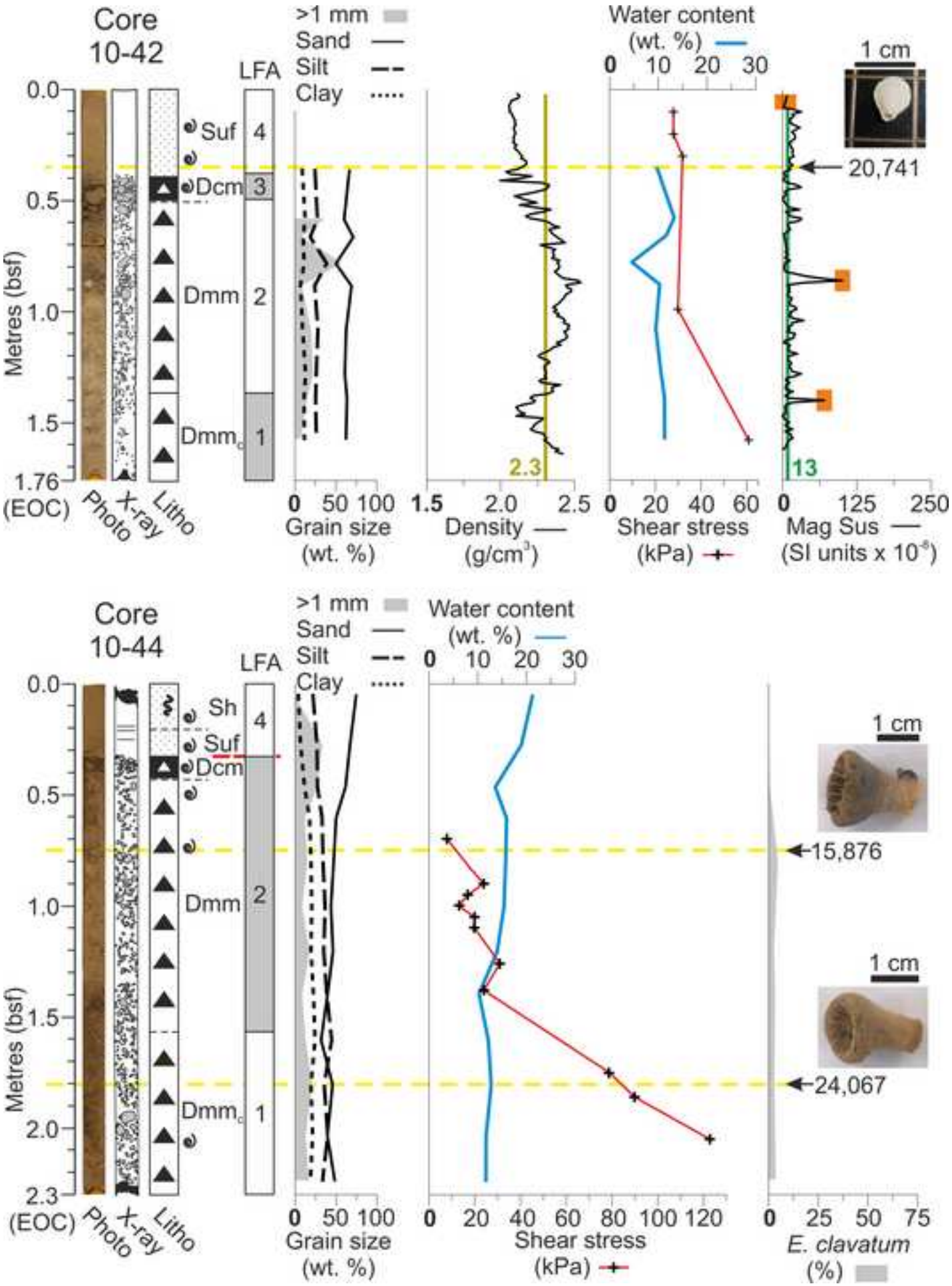

Figure

Click here to download high resolution image

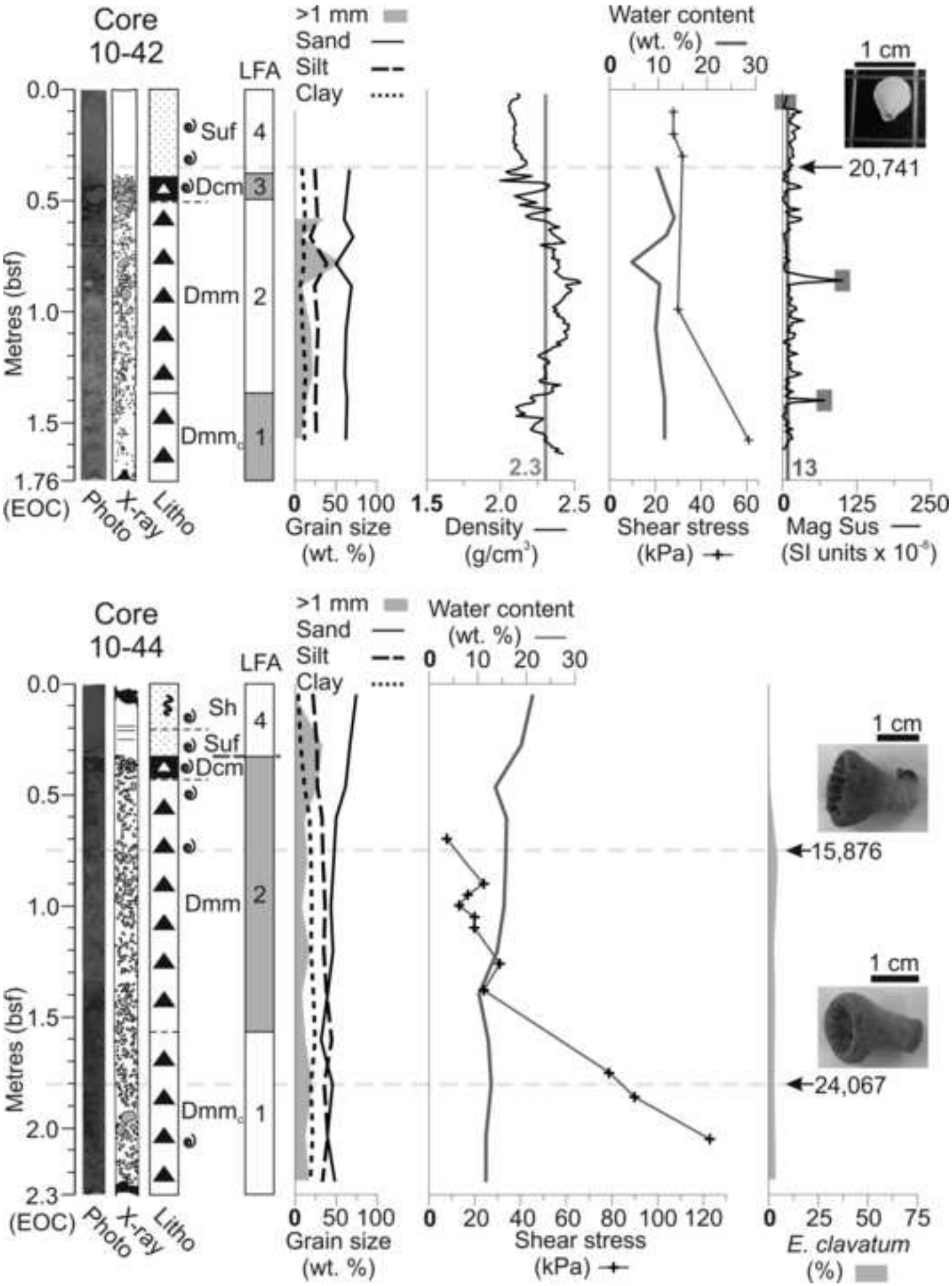

Figure

Click here to download high resolution image

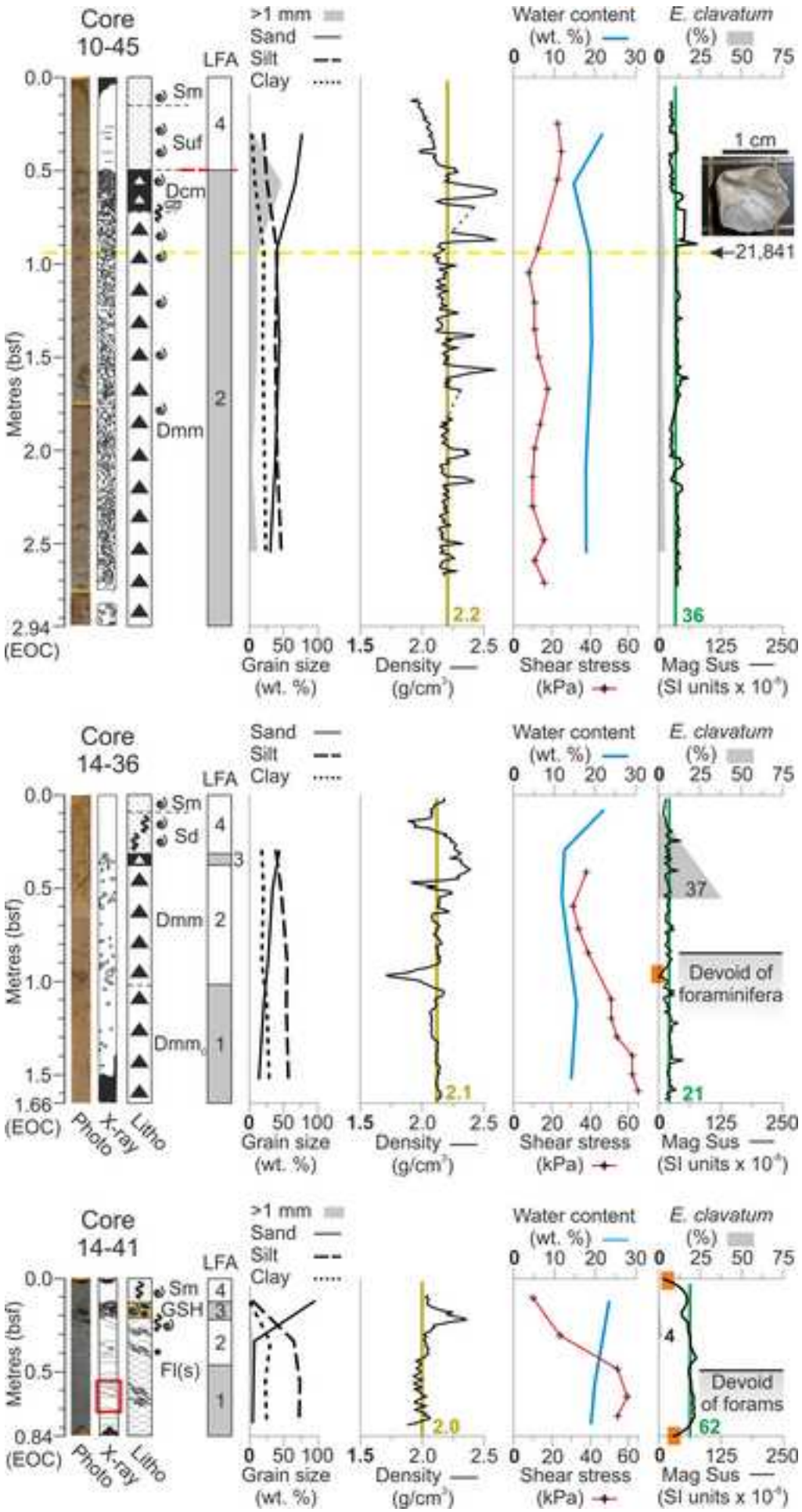

Figure

Click here to download high resolution image

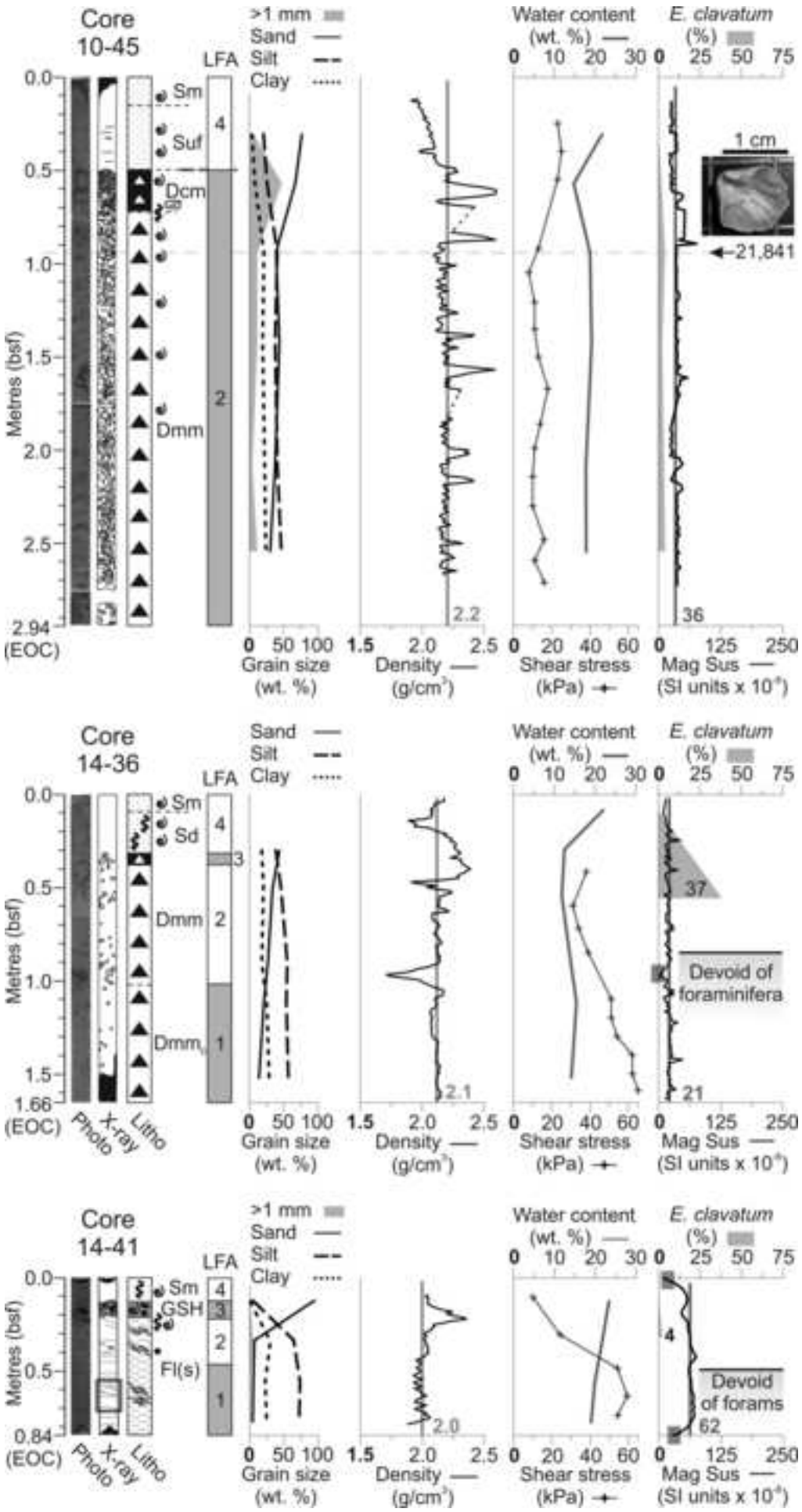

Figure

Click here to download high resolution image

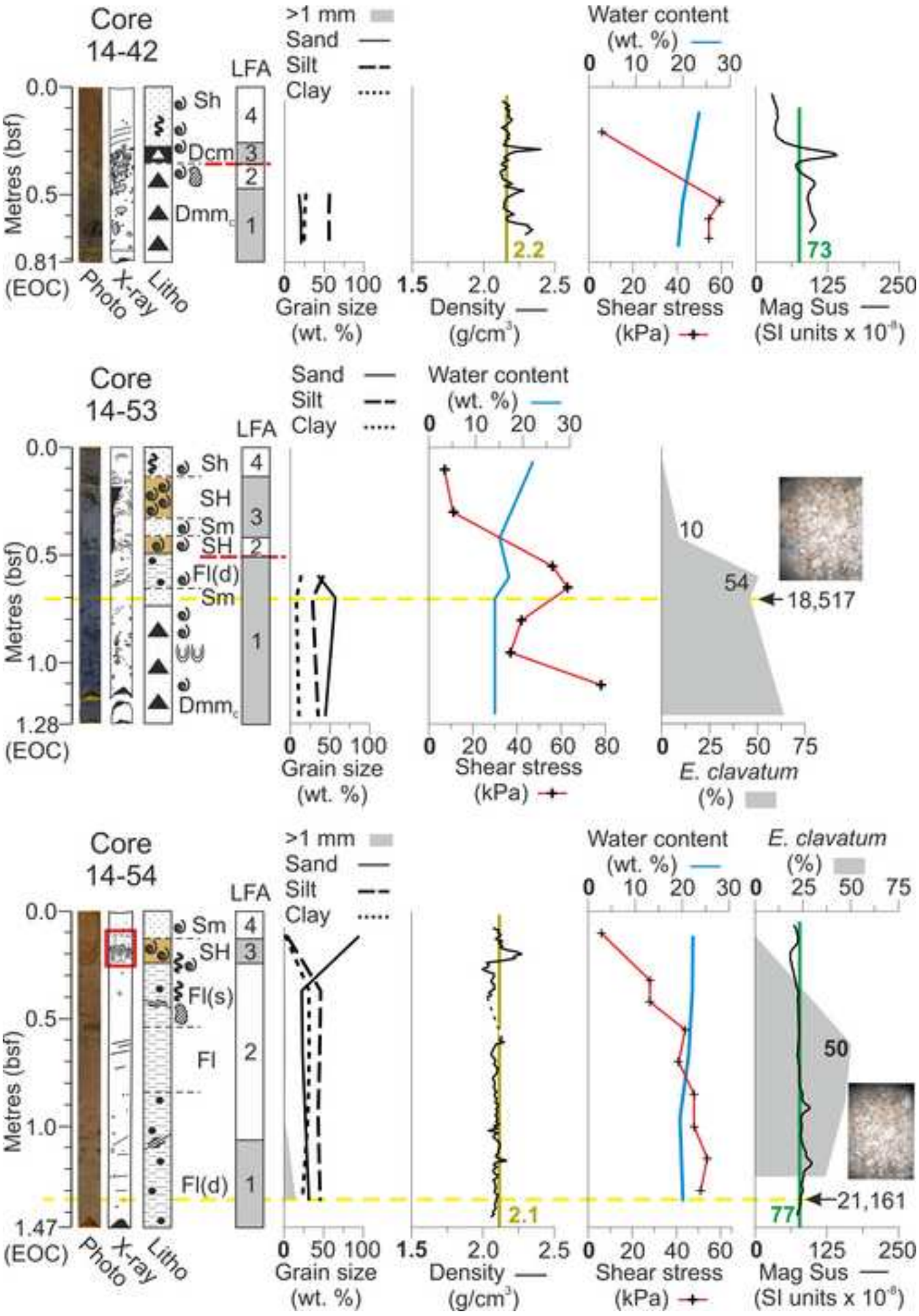

Figure

Click here to download high resolution image

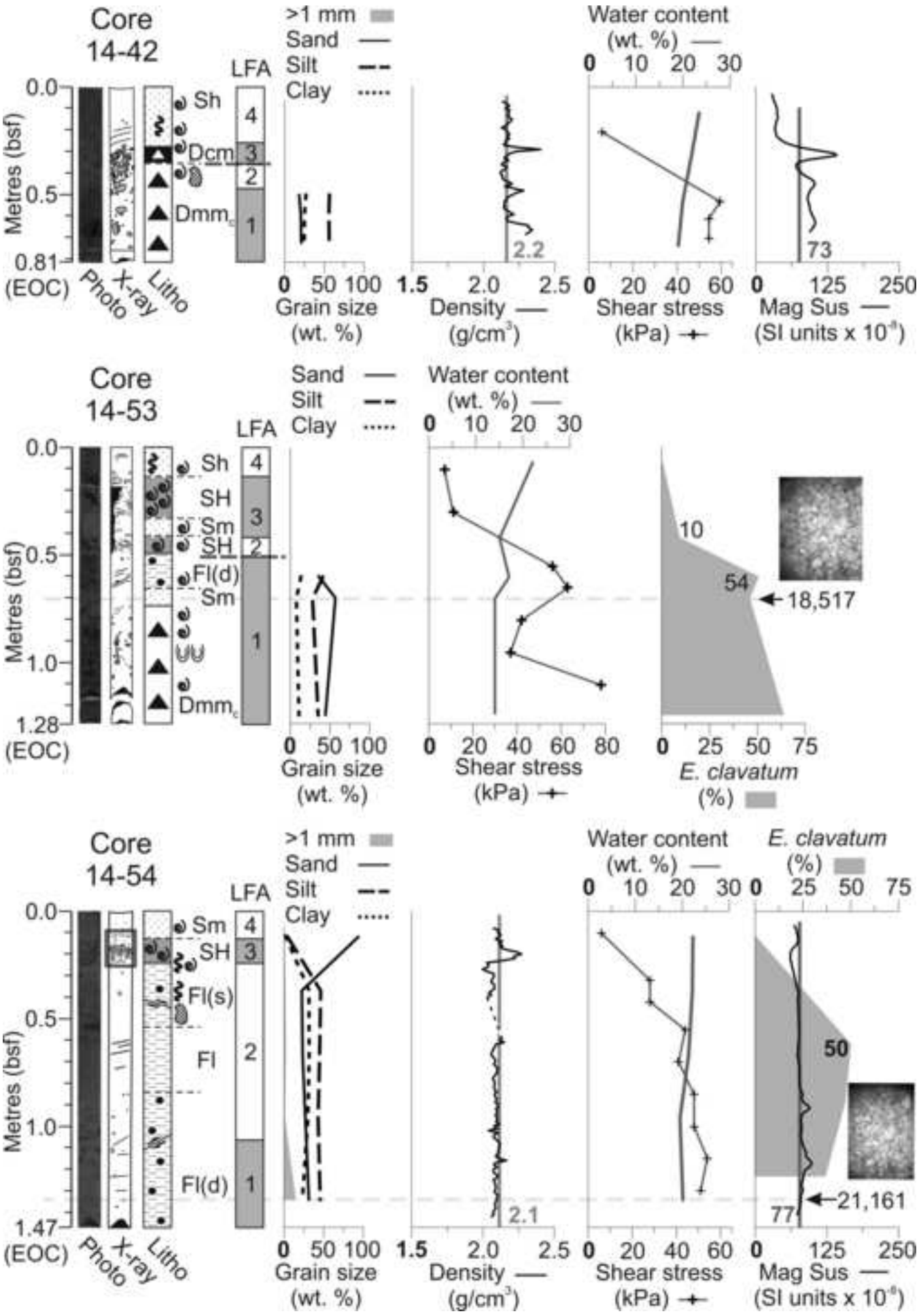

Figure

Click here to download high resolution image

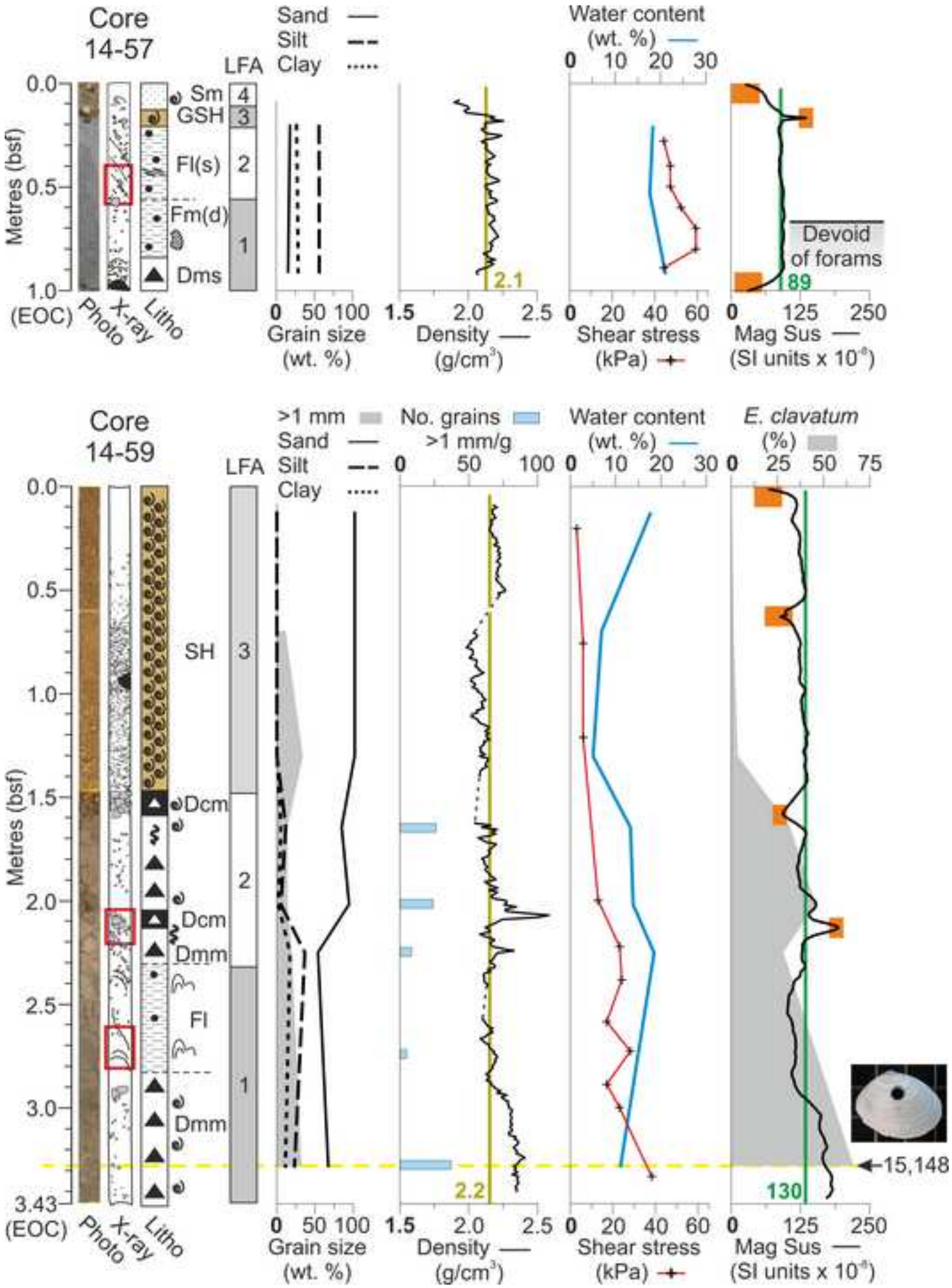

Figure

Click here to download high resolution image

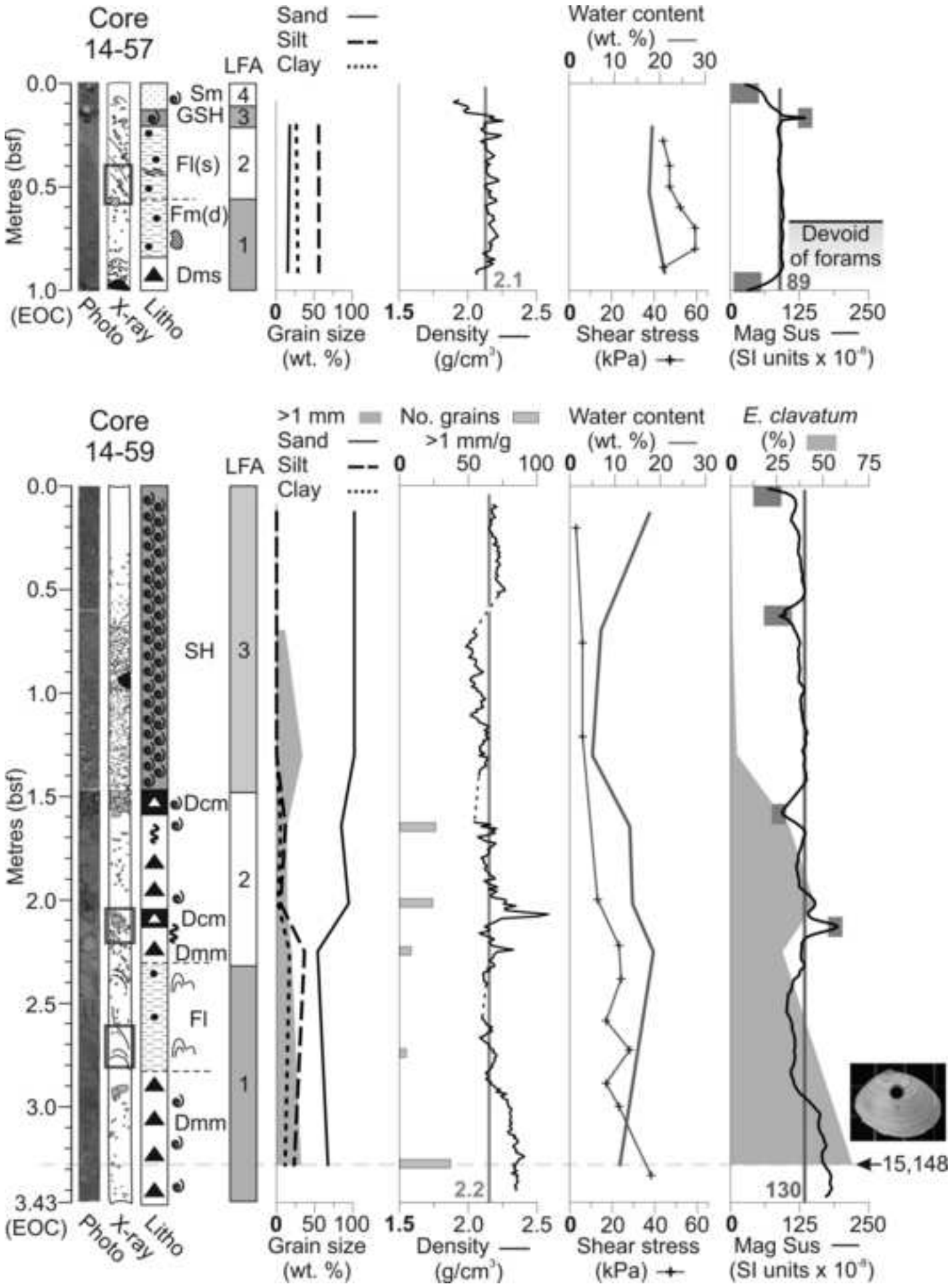

Figure

Click here to download high resolution image

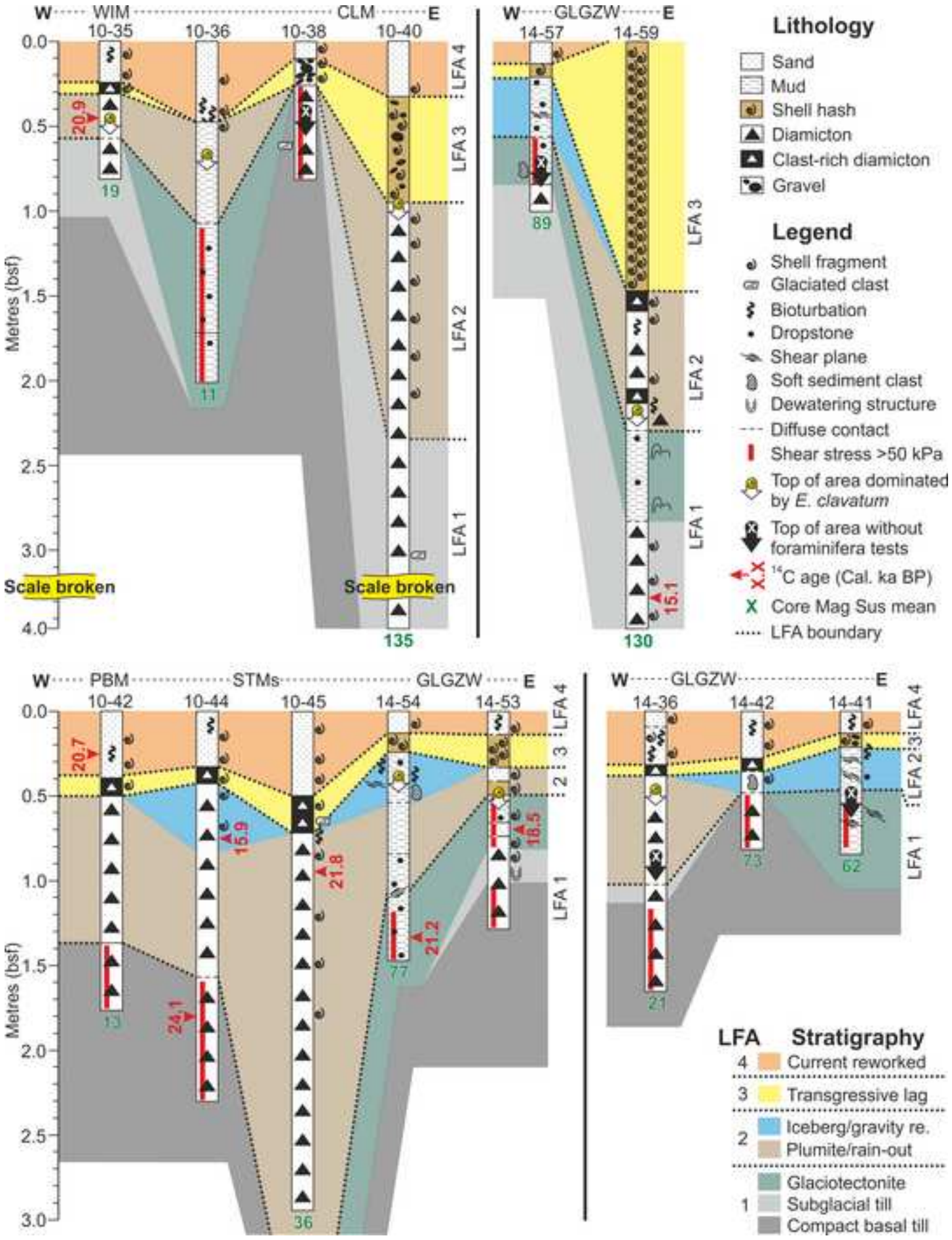

Figure

Click here to download high resolution image

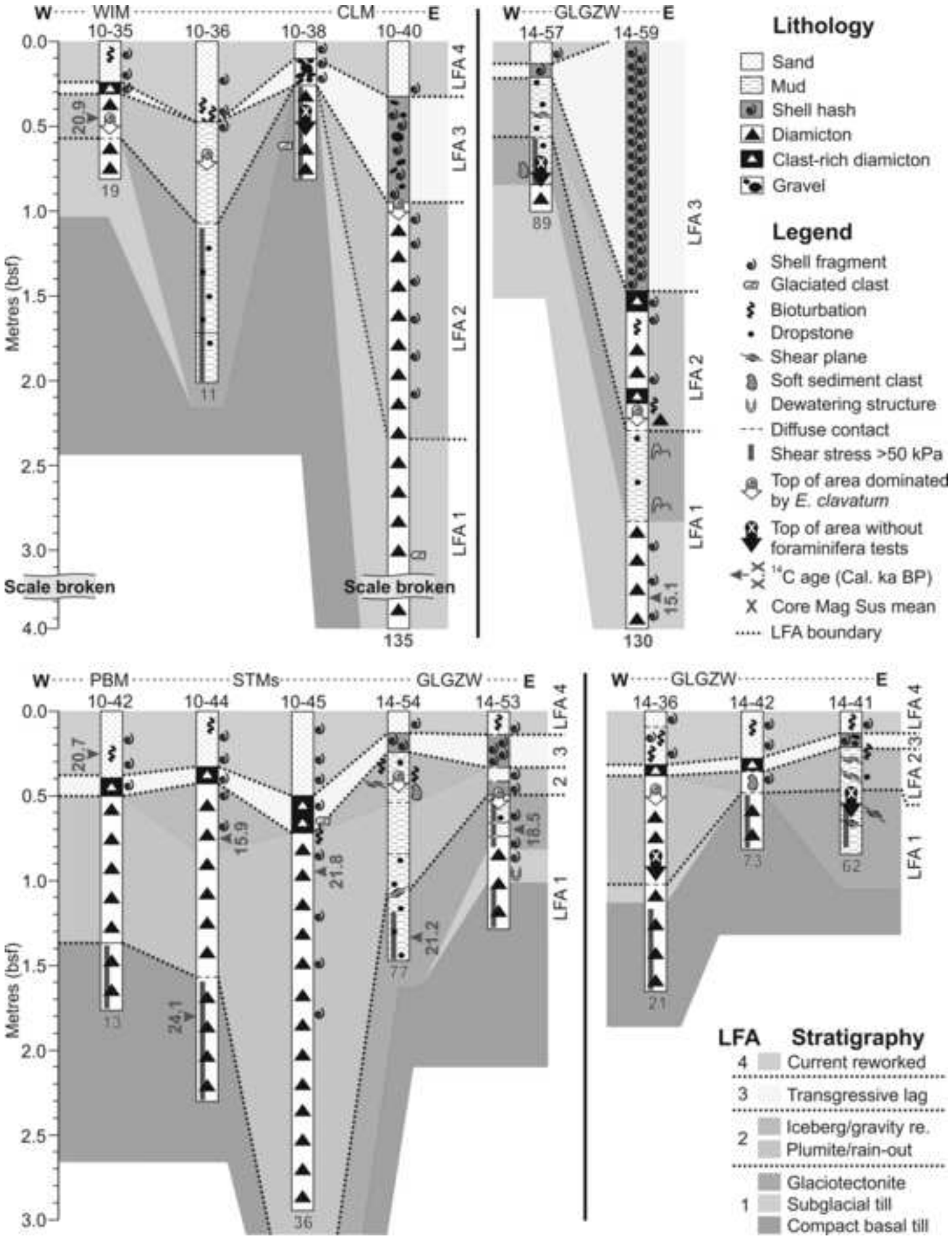

Figure

Click here to download high resolution image

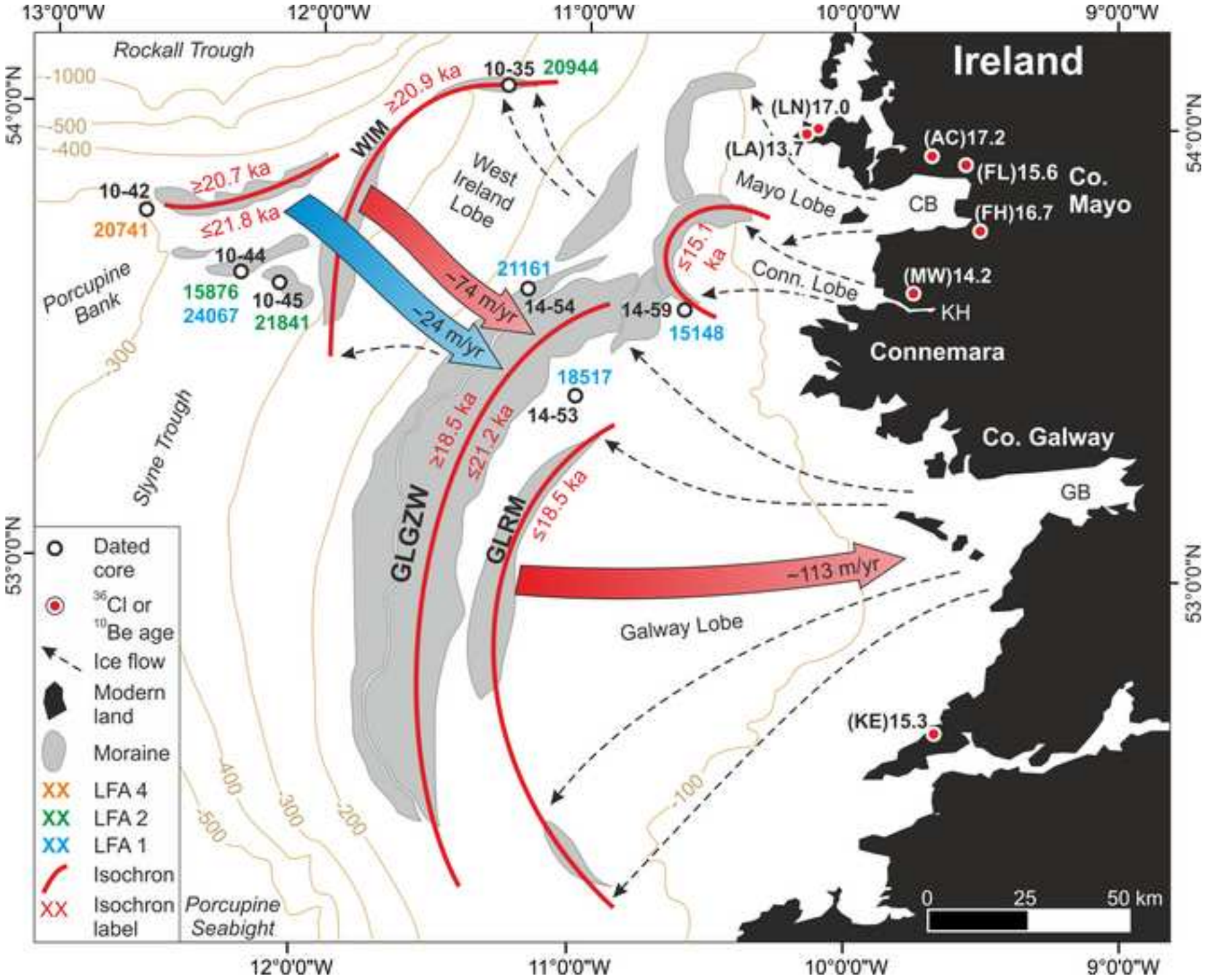

Figure

Click here to download high resolution image

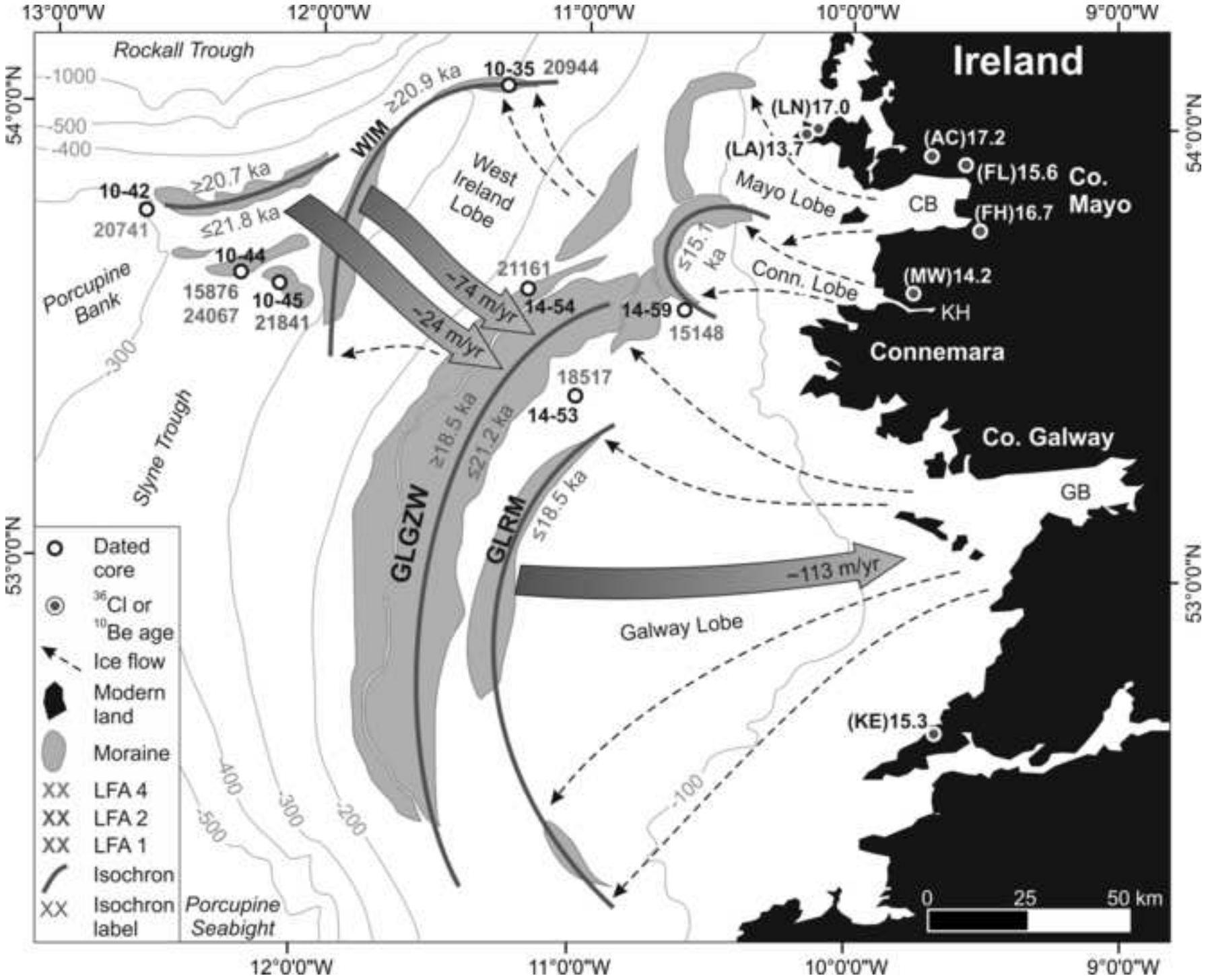

Highlights

Our findings characterise BIIS behaviour during retreat.

New radiocarbon ages constrain retreat rates.

Multiple lines of evidence identify a mid-shelf stillstand.

Geomorphology identifies retreat phase thinning and reconfiguration.

Ice shelf buttressing slowed initial grounding zone retreat.